UC Berkeley
UC Berkeley Previously Published Works

Title

Genome-Resolved Metagenomics and Detailed Geochemical Speciation Analyses Yield New Insights into Microbial Mercury Cycling in Geothermal Springs.

Permalink

https://escholarship.org/uc/item/2hh7z9gq

Journal

Applied and Environmental Microbiology, 86(15)

ISSN

0099-2240

Authors

Gionfriddo, Caitlin M
Stott, Matthew B
Power, Jean F
et al.

Publication Date

2020-07-20

DOI

10.1128/aem.00176-20

Peer reviewed

Genome-Resolved Metagenomics and Detailed Geochemical Speciation Analyses Yield New Insights into Microbial Mercury Cycling in Geothermal Springs

Caitlin M. Gionfriddo,a* Matthew B. Stott,b* Jean F. Power,b Jacob M. Ogorek,c David P. Krabbenhoft,c Ryan Wick,d* Kathryn Holt,d* Lin-Xing Chen,e Brian C. Thomas,e Jillian F. Banfield,a,e,f John W. Moreaua*

aSchool of Earth Sciences, The University of Melbourne, Parkville, Victoria, Australia
bGNS Science, Wairakei Research Centre, Taupo, New Zealand
cWisconsin Water Science Center, U.S. Geological Survey, Middleton, Wisconsin, USA
dDepartment of Biochemistry and Molecular Biology, Bio21 Molecular Science and Biotechnology Institute, University of Melbourne, Parkville, Victoria, Australia
eDepartment of Earth and Planetary Science, UC Berkeley, Berkeley, California, USA
fDepartment of Environmental Science, Policy, and Management, UC Berkeley, Berkeley, California, USA

ABSTRACT Geothermal systems emit substantial amounts of aqueous, gaseous, and methylated mercury, but little is known about microbial influences on mercury speciation. Here, we report results from genome-resolved metagenomics and mercury speciation analysis of acidic warm springs in the Ngawha Geothermal Field ($<55°C$, pH <4.5), Northland Region, Aotearoa New Zealand. Our aim was to identify the microorganisms genetically equipped for mercury methylation, demethylation, or Hg(II) reduction to volatile Hg(0) in these springs. Dissolved total and methylated mercury concentrations in two adjacent springs with different mercury speciation ranked among the highest reported from natural sources (250 to 16,000 ng liter^{-1} and 0.5 to 13.9 ng liter^{-1}, respectively). Total solid mercury concentrations in spring sediments ranged from 1,274 to 7,000 μg g^{-1}. In the context of such ultrahigh mercury levels, the geothermal microbiome was unexpectedly diverse and dominated by acidophilic and mesophilic sulfur- and iron-cycling bacteria, mercury- and arsenic-resistant bacteria, and thermophilic and acidophilic archaea. By integrating microbiome structure and metagenomic potential with geochemical constraints, we constructed a conceptual model for biogeochemical mercury cycling in geothermal springs. The model includes abiotic and biotic controls on mercury speciation and illustrates how geothermal mercury cycling may couple to microbial community dynamics and sulfur and iron biogeochemistry.

IMPORTANCE Little is currently known about biogeochemical mercury cycling in geothermal systems. The manuscript presents a new conceptual model, supported by genome-resolved metagenomic analysis and detailed geochemical measurements. The model illustrates environmental factors that influence mercury cycling in acidic springs, including transitions between solid (mineral) and aqueous phases of mercury, as well as the interconnections among mercury, sulfur, and iron cycles. This work provides a framework for studying natural geothermal mercury emissions globally. Specifically, our findings have implications for mercury speciation in wastewaters from geothermal power plants and the potential environmental impacts of microbially and abiotically formed mercury species, particularly where they are mobilized in spring waters that mix with surface or groundwaters. Furthermore, in the context of thermophilic origins for microbial mercury volatilization, this report yields new insights into how such processes may have evolved alongside microbial mercury methylation/demethylation and the environmental constraints imposed by the geochemistry and mineralogy of geothermal systems.

Address correspondence to Caitlin M. Gionfriddo, gionfriddocm@ornl.gov.

* Present address: Caitlin M. Gionfriddo, Oak Ridge National Laboratory, Biosciences Division, Oak Ridge, Tennessee, USA; Matthew B. Stott, School of Biological Sciences, University of Canterbury, Christchurch, New Zealand; Ryan Wick, Department of Infectious Diseases, Monash University, Melbourne, Australia; Kathryn Holt, Department of Infectious Diseases, Monash University, Melbourne, Australia, and London School of Hygiene & Tropical Medicine, London, United Kingdom; John W. Moreau, School of Geographical and Earth Sciences, University of Glasgow, Glasgow, United Kingdom.

Geothermal springs and fumaroles emit substantial amounts of aqueous and gaseous mercury (Hg) (1). Aqueous Hg concentrations in these systems often exceed 100 ng liter^{-1}, and total Hg levels can approach 25 μg liter^{-1} (2–4). Despite these ultrahigh mercury levels, few studies have examined biotic and abiotic mechanisms for Hg transformations or Hg speciation in geothermal springs. Specifically, the potential for native thermophiles to mediate mercury transformations, i.e., reduction of Hg(II) to Hg(0) or methylation/demethylation of mercury (to CH_3Hg^+ [MeHg] or to Hg[II], respectively) (5–7), remains poorly understood.

Hg species have a high binding affinity to thiols and lipids, causing damage to proteins, enzymes, and nucleic acids. They can inhibit microorganisms at submicromolar concentrations (8). Microorganisms living in environments with elevated Hg (>100 ng liter^{-1}) commonly possess genes encoding Hg resistance (9, 10). The *mer* operon is used by many bacteria and archaea to detoxify Hg(II), by converting it to volatile Hg(0) (7, 10, 11). Interestingly, *mer* has a phylogenetic origin in the thermophiles (12, 13). Additionally, microbes carrying the organomercurial lyase-encoding *merB* gene as part of the *mer* operon are able to detoxify organic Hg compounds, in tandem with mercuric reductase (MerA), to produce methane (CH_4) and Hg(0) (9, 14). Finally, some anaerobic bacteria are suspected to oxidatively demethylate Hg species independent of the *mer* pathway, producing carbon dioxide (CO_2) and Hg(II) (15), although a biochemical pathway has not been identified for *mer*-independent demethylation.

The efficiency of microbial methylation of Hg(II) to MeHg is still largely unknown in geothermal spring ecosystems, particularly under acidic conditions (<55°C, pH <4.5) (4, 5, 16). However, the *hgcAB* genes required by microorganisms to methylate Hg (17) have been reported from many environments, including wetland sediments, rice paddy soils, thawing permafrost, hypersaline and hypersulfidic waters, soda lakes, and geothermal systems (16, 18–20). These environments typically host abundant sulfate- and iron-reducing bacteria (*Deltaproteobacteria*), as well as methanogenic and acetogenic *Methanomicrobia* (*Euryarchaeota*), *Chloroflexi*, and *Firmicutes*, all of which contain species capable of Hg methylation (18, 21–23). Metagenomic analyses have also identified *hgcAB* genes in *Chrysiogenetes*, "*Candidatus* Atribacteria" (candidate phylum OP9), and candidate phylum ACD79 (16). Although Hg methylation is most often associated with sulfate reduction, the existence of environmental triggers or controls on Hg methylation remains poorly understood as does the evolution and phylogenetic distribution of *hgcAB* genes.

By comparison, in nongeothermal environments, elevated Hg concentrations can inhibit microbial Hg methylation (24) and lead to conditions favoring MeHg demethylation (25) or methylation-demethylation cycles (26–28). However, in-depth understanding of Hg methylation in geothermal springs, similarly to acid mine drainage (AMD) (29), has not been established. Conversely, acidophiles in AMD systems have been well studied with respect to potential for metal and sulfur cycling (30), but with less focus on Hg speciation and methylation. Here, we combined metagenomic and geochemical speciation analyses to understand Hg transformations in the context of biogeochemical cycling (e.g., S and Fe) in an acidic warm spring microbiome. To understand physicochemical constraints on microbial Hg transformations, we studied Hg speciation across a gradient of environmental factors that can influence microbiome composition and activity. We compare our findings to those of previous geothermal spring studies to refine the conceptual model for geothermal Hg cycling.

RESULTS

Water and sediment chemistry. Chemical and physical data for each spring are shown in Tables 1 and 2. Chloride concentrations exceeded 400 mg liter^{-1} in all springs

TABLE 1 Anion and cation measurements in filtered water from hot springs in the Ngawha Geothermal Field

Sample site	GPS coordinates (lat, long)	Anion or cation (mg liter^{-1})^a						
		F^-	Cl^-	Br^-	NO_3^-	SO_4^{2-}	S^{2-b}	Fe_T
Tiger Bath (TS1)	−35.4075155°, 173.8554535°	2.1	470	2.79	BDL	1217.8	1.82 ± 0.13	12.7
Cub Bath (TS2)	−35.4075150°, 173.8554755°	1.9	30	0.91	0.74	319.0	6.45 ± 0.15	6.06
Hole to right of Tiger Bath (TS3)	−35.4075160°, 173.8554315°	BDL	395	BDL	BDL	1176.9	0.87 ± 0.47	NM
Hole 3 m from Tiger Bath (TS4)	−35.4075073°, 173.8554202°	BDL	591	BDL	BDL	1017.0	NM	NM
Cinnabar Bath (GN1)	−35.4049290°, 173.8600079°	BDL	876	BDL	BDL	10.2	NM	NM
Jubilee Bath (GN2)	−35.4049108°, 173.8600182°	BDL	1000	BDL	BDL	91.9	NM	NM
Twin Bath (GN3)	−35.4049380°, 173.8600082°	2.6	1073	5.02	BDL	119.9	NM	NM
Kotanitanga (NS1B)	−35.4056976°, 173.8583837°	BDL	661	BDL	BDL	155.1	NM	NM
Adjacent to Favourite Bath (NS3B)	−35.4055000°, 173.8583547°	BDL	639	BDL	BDL	192.5	NM	NM
Waikato Bath (NS4B)	−35.4055887°, 173.8584129°	BDL	537	BDL	BDL	54.1	NM	NM

^{a}NM, not measured; BDL, below detection limit (0.0005 mg liter^{-1}).
^{b}S^{2-} is indicative of all reduced sulfide species.

except Cub Bath (TS2) at 29.8 mg liter^{-1}. Across the Ngawha Geothermal Field (NGF), sulfate concentrations varied from 9.3 to 1,200 mg liter^{-1}, with the highest concentrations found in springs of pH <4 (Table 1). In Tiger Springs (TS), Cub Bath had the lowest sulfate concentration (319 mg liter^{-1}), while those at the other TS sites were >1,000 mg liter^{-1}. Sulfide concentrations were nearly 3.5× higher in Cub Bath (6.45 mg liter^{-1}) than in Tiger Bath (TS1) (1.82 mg liter^{-1}). The total iron concentration in Tiger Bath (12.7 mg liter^{-1}) in October 2011 was twice that of Cub Bath (6.06 mg liter^{-1}).

Total Hg (Hg_T) and total MeHg ($MeHg_T$) measurements of filtered waters from NGF hot springs sampled in April 2011 are shown in Table 2. In comparison to background levels for freshwater systems, Hg_T was relatively high at ~250 to 16,000 ng liter^{-1} compared to 0.4 to 74 ng liter^{-1} for nongeothermal lakes and 1 to 7 ng liter^{-1} for rivers and streams (31). Nonthermal waters in the Ngawha region are reported to contain 300 to 500 ng liter^{-1} Hg (32). Previously reported values for dissolved Hg in NGF thermal waters range from 1,000 to 350,000 ng liter^{-1} (32). In this study, the highest levels of Hg_T were found in the Tiger Springs region (all >1,000 ng liter^{-1}) and from Cinnabar Bath (GN1) in the Ginn Ngawha Spa (1,460 ng liter^{-1}) (see Fig. S3 in the supplemental material). Methylmercury levels ranged from 0.5 to 14.0 ng liter^{-1}; however, elevated concentrations of $MeHg_T$ did not correlate with higher Hg_T concentrations. Concentrations of Hg_T and $MeHg_T$ in filtered water samples from NGF were compared to reference values (Table 2). MeHg levels in filtered water samples from Yellowstone National Park (YNP) were substantially lower than those observed at NGF, with most YNP springs having concentrations below the detection limit (0.013 ng liter^{-1}). Those with detectable MeHg were still relatively low at 0.026 to 0.080 ng liter^{-1} (5). Only three sites sampled in the NGF exhibited a significant proportion of Hg_T as MeHg (~1% [vol/vol]): Cub Bath (TS2), Kotanitanga Bath (NS1B), and a drainage pool adjacent to Favourite Bath (NS3B). Methylmercury levels were nearly an order of magnitude greater in Cub Bath (TS2) than in Tiger Bath (TS1), even though the total mercury levels were roughly the same (~1,000 ng liter^{-1}).

Sediments collected from the Tiger Springs area in October 2011 were analyzed for Hg_T (Table 2). Total Hg concentrations were highest in the hole adjacent to Tiger Bath (TS3) at ~7,000 μg g^{-1}. Tiger Bath (TS1) sediments had approximately one-half the solid Hg_T of TS3, at 3,467 μg g^{-1}, and Cub Bath sediments had approximately one-third the solid Hg_T of Tiger Bath (1,274 μg g^{-1}). Gaseous Hg(0) emissions were also recorded from the baths (Table 2). The Hg(0) concentration measured above Tiger Bath (25.0 ng liter^{-1}) was greater than that of Cub Bath (4.34 ng liter^{-1}) but also varied across the bath (4.38 to 25.0 ng liter^{-1}). Furthermore, these values are an order of magnitude lower than previously reported concentrations of fumarolic Hg(0) in the Tiger Springs area at 13.5 to 276 μg liter^{-1} and 710 μg liter^{-1} from Tiger Bath specifically (32).

Microbial diversity from metagenomic data sets. Phylogenetic analysis of ribosomal marker protein S3 from assembled Tiger and Cub Bath metagenomes identified members of *Deltaproteobacteria*, *Gammaproteobacteria*, *Thermotogae*, "*Candidatus* Mi-

TABLE 2 Mercury analyses of NGF hot springs

Location (reference)	Water temp (°C)[b]	pH[b]	MeHg[c] (ng liter^{-1})	Hg$_T$[d] (ng liter^{-1})	% MeHg$_T$ of Hg$_T$[e]	THg$_{(s)}$[f] (μg g^{-1})	Hg(0)[g] (ng liter^{-1})
NGF[a] (this study)							
Tiger Bath, TS1	35.3–40.5	2.9–3.0	1.56	1,031	0.15	3,467	25
Cub Bath, TS2	24.5–33.4	3.6–3.2	13.9	1,042	1.33	1,274	4.3
Hole to right of Tiger Bath, TS3	35.9–40.3	2.9–3.8	4.33	16,711	0.03	7,000	7.5
Hole 3 m from Tiger Bath, TS4	21.6	3.96	0.53	2,160	0.02		
Cinnabar Bath, GN1	40.4	6.72	5.36	1,461	0.37		
Jubilee Bath, GN2	38	6.45	1.28	244	0.52		
Twin Bath, GN3	34.1	6.44	1.61	722	0.22		
Kotanitanga, NS1B	32.4	6.54	4.28	487	0.88		
Adjacent to Favourite Bath, NS3B	26.5	7.14	3.57	253	1.41		
Waikato Bath, NS4B	45.5	6.7	0.90	326	0.28		
Regional values[h]							
NGF soils and waters (32)				17,000–710,000		0.017–0.35	2,000–78,500
Tiger Bath (32)	32–57	5–8		710,000			
NGF nonthermal waters (32)				300–500			
Puhipuhi mine waters (68)			0.61–1.02	69.6–240	0.3–1.6	35–1,748	0.06–0.50
Wairua River, Northland (84)				100–1,000		<100	
YNP[i]							
Nymph Lake spring no. 1 (5)			0.026	170	0.02		
Nymph Lake spring no. 2 (5)			0.43	520	0.08		
Roadside West Spring (5)	65	6.4	0.08	200	0.04		
Thermal waters and microbial mats (5)	36.4–80	2.2–8.6	<0.013–0.43	15–520		0.0049–120	
Acidic thermal springs (6)			<0.025	38–94			
Acidophilic microbial mats (6)			0.03–1.62	2–71		0.16–18	
Filtered thermal waters and microbial mats (7)	21.9–74.4	1.8–9.3		7.3–144		0.38–20.52	
Reference standards and values[h]							
North American lakes (31, 85)			0.003–6	0.04–74	8.11		
North American rivers and streams (31, 85)			0.078–0.55	1–7	7.86		
NZ drinking water standard				7,000			
US EPA, acute aquatic life water standard				2,400			
US EPA, chronic aquatic life water standard				770			

[a]NGF, Ngawha Geothermal Field.
[b]Measurements taken during each sampling campaign are provided as a range.
[c]MeHg, methylmercury.
[d]Hg$_T$, total mercury.
[e]The fraction of total Hg as MeHg (as %) in filtered water samples.
[f]THg$_{(s)}$, solid total mercury in hot spring sediments.
[g]Hg(0), gaseous elemental mercury above the springs.
[h]Published reference and regional background values are included for comparison.
[i]YNP, Yellowstone National Park.

crarchaeota," "*Candidatus* Parvarchaeota," *Thermoplasmata*, and other *Euryarchaeota* (see Fig. S4 and S5). Furthermore, phylogenetic analysis revealed a greater breadth in the phyla of genomes resolved from Cub Bath compared to that from Tiger Bath, with *Verrucomicrobia*, *Acidobacteria*, *Firmicutes*, *Planctomycetes*, *Alphaproteobacteria*, and *Betaproteobacteria* identified in Cub Bath only (Fig. S4). Ribosomal proteins from *Thermoprotei* were identified only in assembled Tiger Bath metagenomic data (see Fig. S5). Genome binning resulted in acidophilic and thermophilic bacteria and archaea dominating the Tiger and Cub Bath metagenomic data sets, with the average coverage of scaffolded contigs within genome bins ranging from 7.1 to 789× (Fig. 1; Table S2). The highest coverage bins in each bath were related to *Acidithiobacillus*, *Thermotogales*, and *Thermoplasma* (Fig. 1).

Genome bins were comprised of aerobes as well as obligate and facultative anaerobes capable of sulfur oxidation (*Acidithiobacillus* spp. and *Thiomonas*), sulfur reduction (*Desulfurella acetivorans* and *Granulicella mallensis*), iron oxidation (*Ferroplasma* and *Acidithiobacillus ferrivorans*), iron reduction (*Acidobacterium capsulatum*), methane oxidization (*Methylacidiphilum*), and acetate oxidation (*Desulfurella acetivorans*) (Fig. 2). To elucidate important biogeochemical links to Hg cycles mediated by these microbial
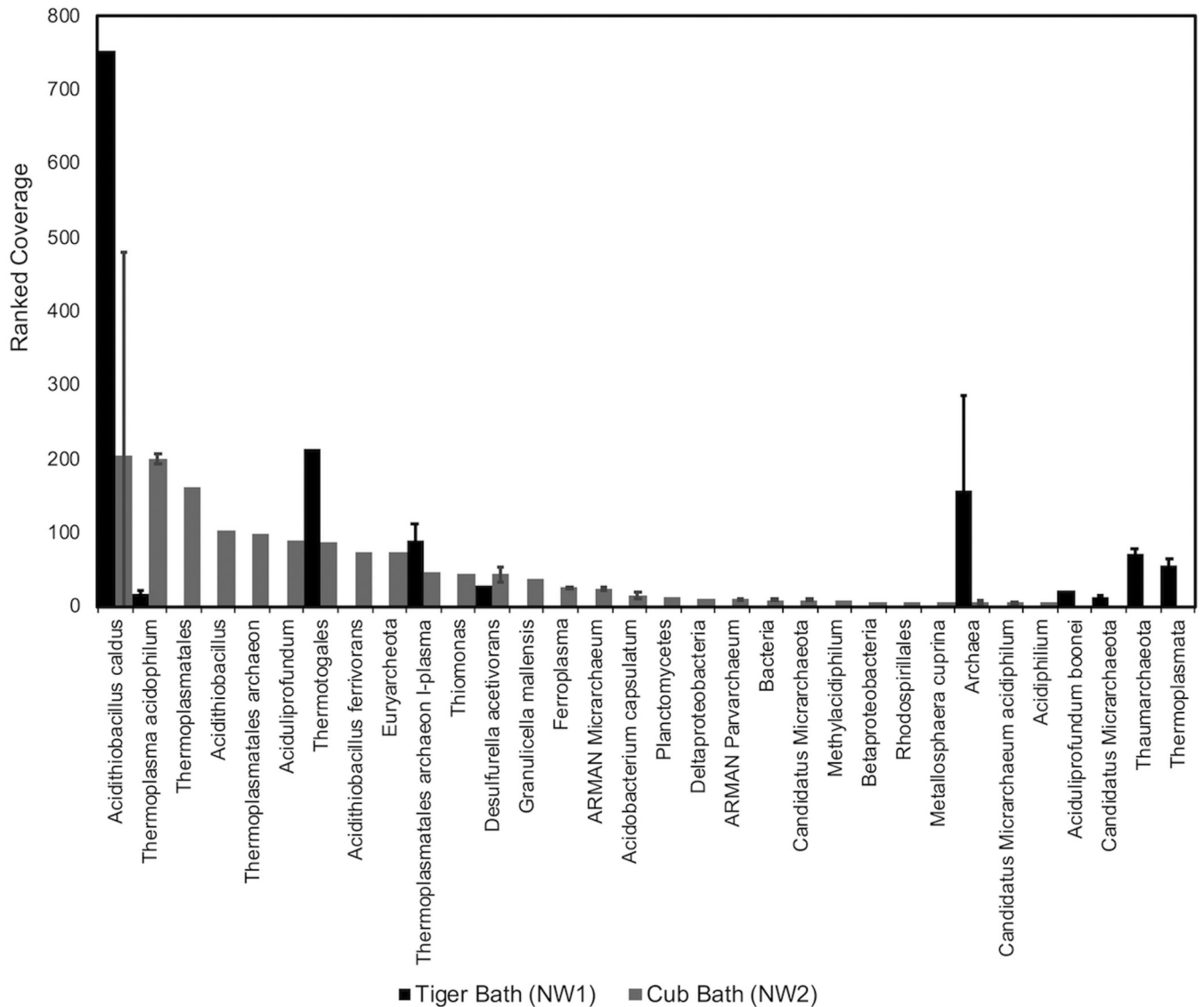
FIG 1 Rank abundance by scaffold coverage of ribosomal protein S3 within binned and unbinned genomes from Tiger (NW1) and Cub (NW2) Bath metagenomes. Analyses and annotations were performed in ggKbase (https://ggkbase.berkeley.edu/). Genomic bin phylogeny used ribosomal S3 proteins from genomic bins, while scaffold phylogeny to the lowest common ancestor is given for unbinned ribosomal proteins. When multiple ribosomal protein S3s had the same taxonomic classification, the average coverage is shown, with error bars representing standard deviations. Values are ranked by NW2 coverage.

phylotypes, metagenomes were searched for genes encoding Hg, sulfur, sulfate, and methane cycling (Fig. 2). We note here that genes involved in methanogenesis (notably *mcrA*) and methane oxidation (*pmoA*) were nearly absent from metagenomes (Fig. 2).

Mer operon. Assembled metagenomes were screened for genes belonging to the *mer* operon that encode mercuric reductase (*merA*), organomercurial lyase (*merB*), a periplasmic protein (*merP*), and inner membrane proteins involved in Hg(II) transport (*merT*, *merC*, *merE*, *merF*, and *merG*), as well as one or more regulatory proteins (*merR* and *merD*) (13). At Ngawha, scaffolded *mer* genes were often encoded in the higher coverage genome bins of each bath, *Acidithiobacillus* spp., *Thiomonas*, and *Thermotogae* (see Table S5; Fig. 2). The coverage of *mer* scaffolds ranged from 3.9 to 836×, with scaffold lengths of 1,021 to 101,352 bp, indicating that a significant number of reads mapped to each sequence. A high fraction of reads (3.24E−04 to 1.94E−04) (see Table S1) from each metagenome were predicted to encode mercuric reductase (MerA) using the hidden Markov model (HMM). BLASTP analysis of HMM search outputs indicated that the HMM was insufficient for filtering sequences that are predicted to encode
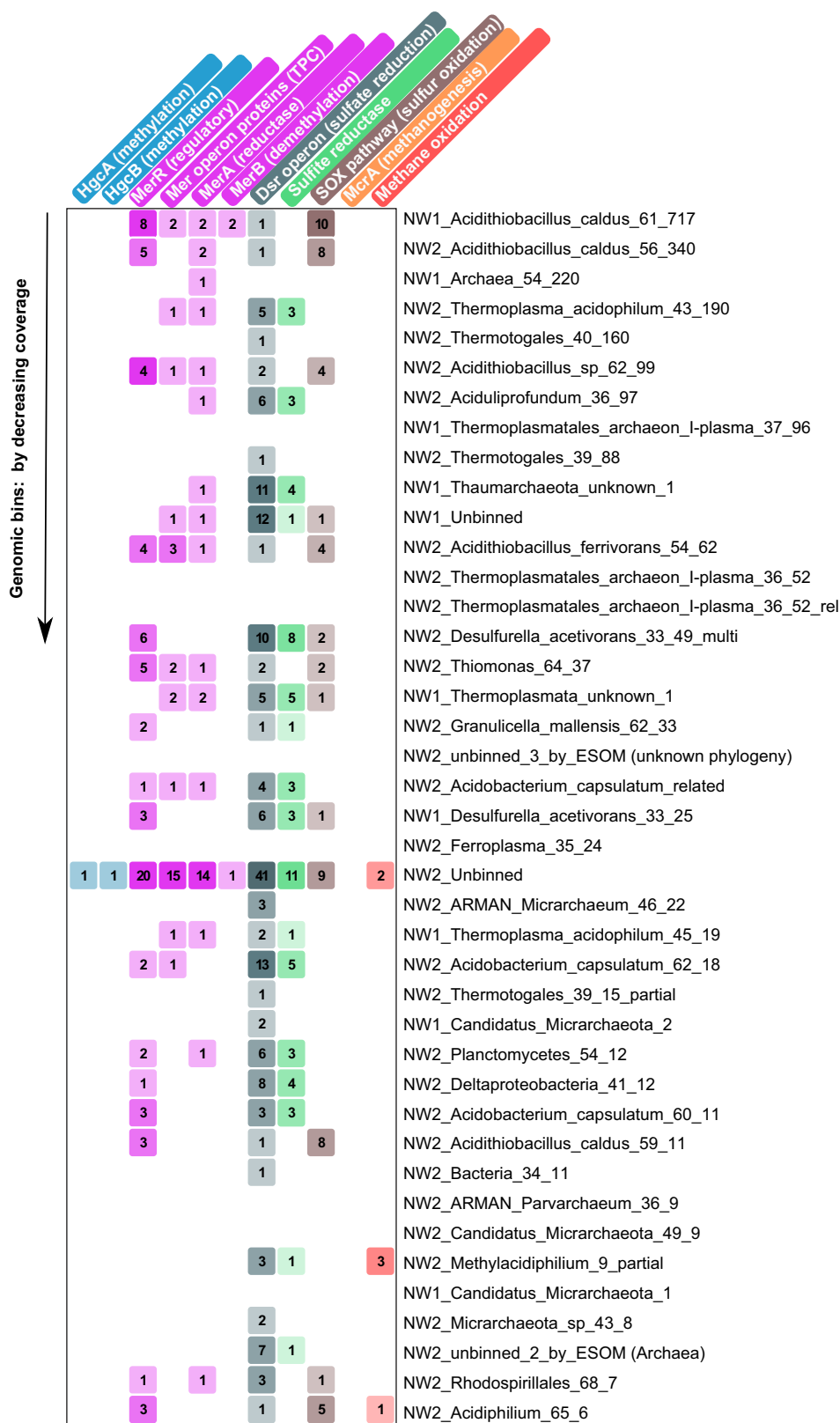
FIG 2 Heat map showing functional proteins from various biogeochemical pathways associated with Hg within genomic bins and unbinned (NGAWHA_1_UNK and NGAWHA_2_UNK) scaffolds from Tiger (NW1) and Cub (NW2) Bath metagenomes. Intensity of color refers to number of genes from each bin that encode the enzyme, operon, or pathway involved in mercury, sulfur, or methane cycling; values are provided in cells for reference. Genomic bins were ordered by the consensus coverage for all scaffolds within the bin (highest to lowest). Analyses and annotations were performed in ggKbase (https://ggkbase.berkeley.edu/).

MerA paralogs dihydrolipoamide dehydrogenase and pyridine nucleotide-disulfide oxidoreductase. Therefore, the HMM likely overestimates MerA abundance encoded by the raw reads. MerA homologues identified in the assembled Tiger and Cub Bath metagenomes using ggKbase annotations were related to both *Archaea* (*Euryarchaeota*) and *Bacteria* (*Proteobacteria* and *Bacteroidetes*) (Fig. 3). Most archaeal MerA were related to *Thermoplasma*; however, four MerA homologues branched deeply from known archaeal homologues and were related (<43%, BLASTP sequence alignment) to MerA from "*Candidatus* Methanoperedens nitroreducens" (NW1 scaffolds 675 and 247, and NW2 scaffolds 1319 and 13696) (Fig. 3). Most MerA homologues from Cub Bath were related to *Acidithiobacillus* spp. (Fig. 3). MerA homologues identified in the metagenomes were from operons also encoding MerP, MerT, and MerR (Table S5). Several scaffolds related to *Euryarchaeota* (*Thermoplasma*) encoded just for MerA and MerP (NW1_scaffold_26, NW1_scaffold_675, and NW2_scaffold_876) (Table S5), consistent with *Thermoplasma mer* genes sequenced from acid mine drainage (AMD) (33).

Two similar but distinct *merB* genes were identified in assembled Tiger and Cub Bath metagenomes, related to *Acidithiobacillus caldus* and *Thioalkalivibrio* spp., respectively (see Fig. S6). The *merB* gene from Tiger Bath (NW1_scaffold_113) was linked to a genome bin identified as *Acidithiobacillus caldus*, with an average scaffold coverage of 750× (Table S5). The same scaffold (NW1_scaffold_113) contained two *merR* genes that were convergent and divergent, respectively, to *mer* genes that encode MerT, MerP, and MerA. The *merB* gene from Cub Bath (NW2_scaffold_17399) was most closely related to *merB* from *Thioalkavibrio* spp.; however, the scaffold itself was unbinned, with an overall taxonomic identification of *Acidithiobacillus ferrivorans* (Table S5). The scaffold also contained *merR* and *merA* genes related to *Acidithiobacillus ferrivorans* (WP_035195121). The translated organomercurial lyases (MerB) from Tiger and Cub Baths aligned to conserved cysteines (34), indicative of their true functionality (see Fig. S7).

Biological Hg methylation. Both Tiger and Cub Bath metagenomic read sets were searched for sequences sharing homology to Hg methylation genes (*hgcA* and *hgcB*) (17). A small fraction of reads (2.16E−07) were identified as fragments of *hgcA* sequences in the Cub Bath metagenome (Table S1). The nucleotide reads were each 100 bp in length and, when translated, aligned to several regions of HgcA from known methylators, including the highly conserved G(I/V)NVWC region of the HgcA protein (17) (see Fig. S8). Several of the reads aligned to one another, and a composite amino acid sequence (59 amino acids [aa] in length) is shown in Fig. S8. Phylogenetic analyses of the translated reads revealed two distinct *hgcA*-like genes in the Cub Bath metagenome (Fig. 4). One of the reads closely matched (BLASTP search) to pterin-binding regions of HgcA-like proteins from marine bacteria *Streptomyces* sp. CNQ-509 and *Nitrospina* spp. (E value, 8E−05; 93% sequence coverage, 55%) and to fused HgcAB proteins primarily found in thermophilic archaeal and bacterial genomes, *Thermococcus* sp. strain EP1, *Kosmotoga pacifica*, *Pyrococcus furiosus*, and *Methanococcoides methylutens* (E values, 3E−06 to 8E−08; 100% sequence coverage, 65% to 75% sequence identification [ID]). Whether these microbes with genomes encoding an HgcAB fused protein are capable of Hg methylation is unknown (16). When tested for Hg methylation capability, both *Pyrococcus furiosus* and *Methanococcoides methylutens* were unable to produce MeHg at levels higher than controls (16, 35).

The second set of *hgcA* reads from Cub Bath (reads 2 to 7) (Fig. 4), including the composite sequence, were aligned using BLASTP to the pterin-binding region of HgcA proteins from known and predicted Hg methylators *Desulfosporosinus youngiae*, *Clostridium cellobioparum*, *Desulfosporosinus* sp. strain Tol-M, and *Desulfosporosinus* sp. BRH-c37 (E values, 4E−21 to 7E−22; 100% query cover; 71 to 75% ID). Phylogenetic analyses (Fig. 4) of the composite sequence revealed homology to HgcA from *Nitrospirae* bacterium HCH-1 (GenBank ID LNQR00000000.1) and to HgcA from hot spring metagenomes. The Cub Bath *hgcA* sequences could not be binned; therefore, additional taxonomic information about *hgcA* carrying genomes was not obtained. Taxo-
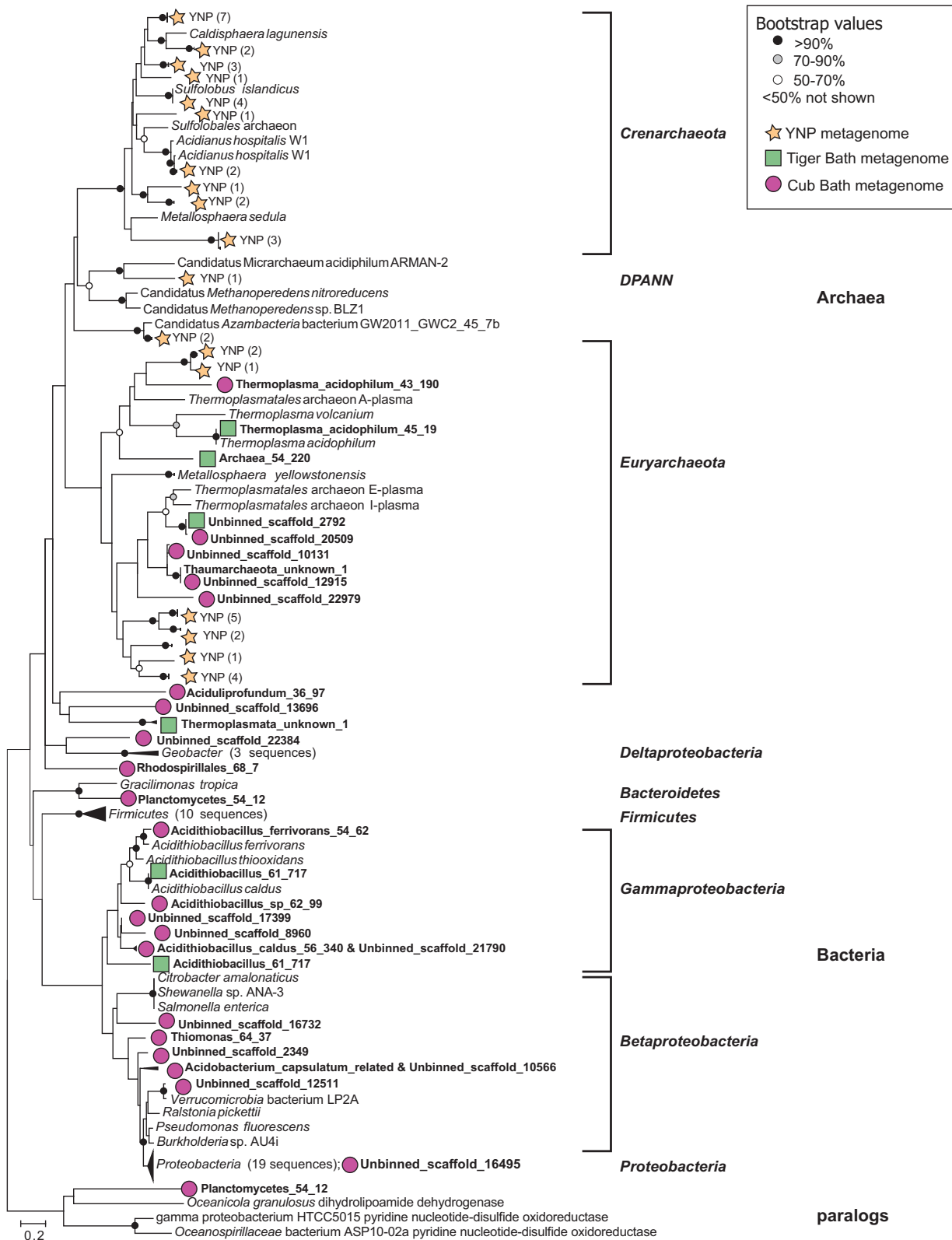
FIG 3 Maximum likelihood tree showing MerA phylogeny of 31 sequences pulled from assembled Tiger (NW1) and Cub (NW2) Bath metagenomes using ggKbase. Genomic bins or scaffold ID (when MerA was unbinned) are given in bold font. Included in analysis are 113 MerA homologues, including 46 sequences from Yellowstone National Park (YNP) metagenomes (82). Trees were constructed using Le Gascuel amino-acid substitution model with gamma distribution in MEGA6 (77). Data were bootstrapped with 100 replications. The initial neighbor-joining tree was constructed with pairwise distances estimated using a JTT model. Positions with less than 90% site coverage (e.g., alignment gaps, missing data, or ambiguous bases) were excluded. A total of 419 positions were used in the final data set.
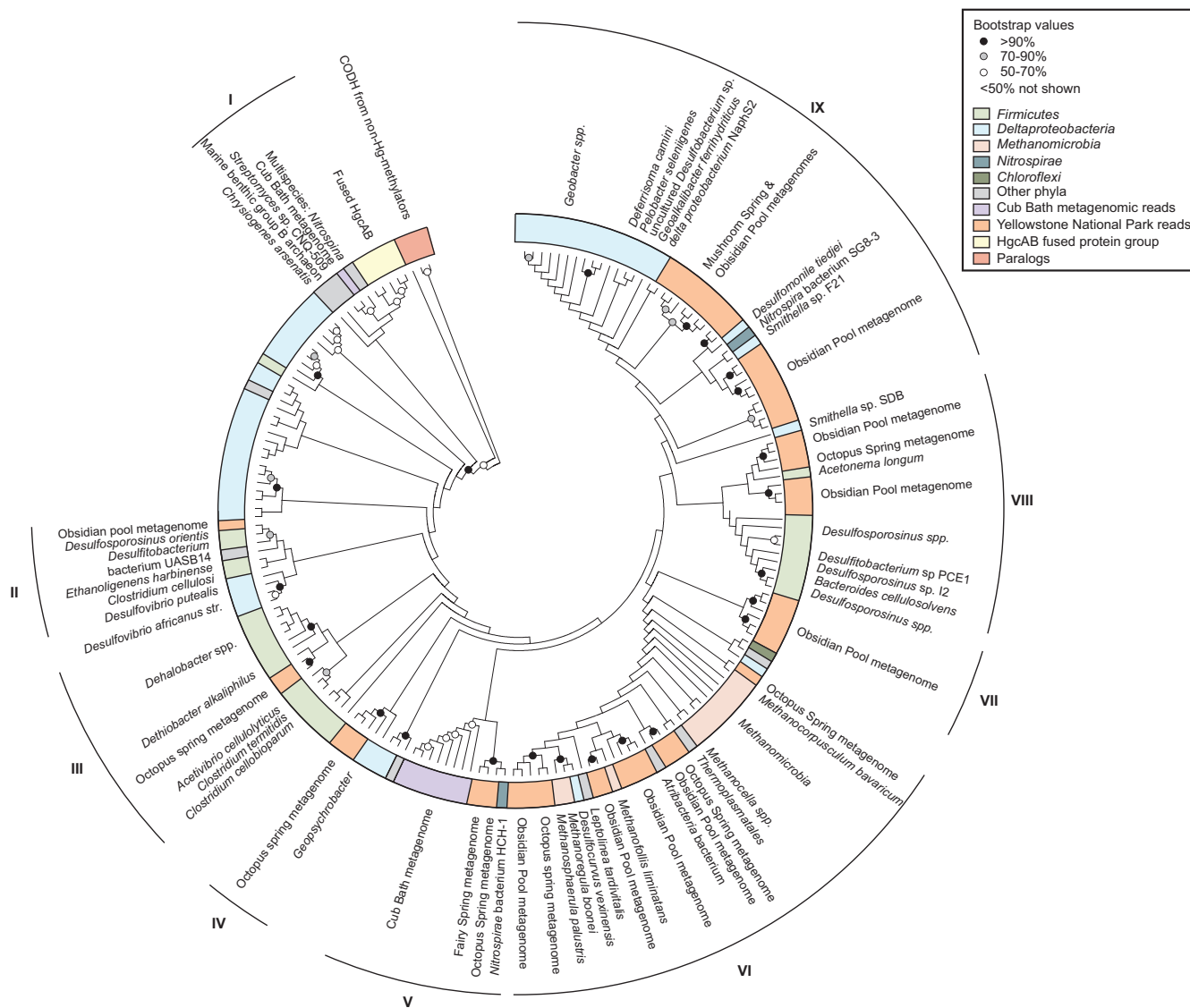
FIG 4 Maximum likelihood tree showing HgcA phylogeny of reads obtained from the Cub Bath (NW2) metagenome using HMM search. Included in analysis are 183 sequences, including 56 HgcA homologues from YNP metagenomes, pulled from JGI (see Table S3 in the supplemental material). Amino acid sequences are compared to HgcA homologues from known and predicted methylators. Also included are HgcAB fused proteins from hyperthermophilic bacteria and archaea and carbon monoxide dehydrogenase/acetyl coenzyme A (acetyl-CoA) synthase subunit gamma (HgcA paralogs) from nonmethylators. Trees were inferred from the Le Gascuel amino acid substitution model with gamma distribution in MEGA6 (77). Data were bootstrapped with 100 replications. The initial neighbor-joining tree was constructed with pairwise distances estimated using a JTT model. Positions with less than 93% site coverage (e.g., alignment gaps, missing data, or ambiguous bases) were excluded. A total of 55 positions were used in the final data set. Groups (I to IX) designate distinct subtrees that contain HgcA from hot spring metagenomes. Representative reference sequences are labeled within each subtree, while phylogeny of all branches is indicated by color.

nomic assignments of Hg methylators from HgcA phylogeny alone are not conclusive. The *hgcA* sequences pulled from assembled YNP and British Columbia hot spring metagenomes from JGI-IMG databases span a wide range of diverse phyla and are predicted to encode HgcAs that relate closely to those from *Deltaproteobacteria*, *Firmicutes*, *Nitrospirae*, *Planctomycetes*, and *Euryarchaeota* (*Methanomicrobia* and *Thermoplasmata*) (Fig. 4). BLASTP searches of translated amino acid sequences revealed common closest matches (<83% ID) to *Clostridium straminisolvens*, *Deltaproteobacterium* sp. NaphS2, *Nitrospirae* bacteria SG8-3 and HCH-1, *Phycisphaerae* bacterium SG8-4, *Smithella* spp., *Methanocella arvoryzae*, and *Thermoplasmatales* archaeon DG-70-1. Of these closest relatives, only *Thermoplasmatales* archaeon DG-70-1 is from a thermophilic phylum (*Thermoplasmata*); however, this strain was isolated from an anaerobic, moderately halophilic, and mesophilic aquatic environment (36) rather than a geothermal spring.

A high fraction of reads from each metagenome aligned to *hgcB* sequences from known and predicted methylators (2.08E−06 to 3.02E−06) (Table S1). However, BLAST analysis of the translated *hgcB*-like genes resulted in closest matches to ferredoxin-encoding gene sequences in both Tiger and Cub Bath. To differentiate between other ferredoxin proteins and HgcB homologues, the translated *hgcB*-like genes were searched for the conserved C(M/I)ECGAC site in HgcB (17). A complete *hgcB* gene was identified in the assembled Cub Bath metagenome (NW2_scaffold_10600_2) (see supplemental material). A translated BLASTP search of the sequence revealed the closest matches (E values, 2E−26 to 3E−29; 91% to 98% coverage; 53% to 57% identity) to HgcB were from predicted Hg methylators *Dehalobacter* spp., *Clostridium straminisolvens*, *Nitrospirae* bacterium HCH-1, and *Syntrophobotulus glycolicus*. Other features on the assembled contig that contains the *hgcB* gene (NW2_idba_contig_10600) include a partial *hgcA* gene upstream from *hgcB*, and downstream genes encode a DsrE/DsrF-like family protein (involved in intracellular sulfur reduction) related to *Planctomycetes*, a copper-binding protein related to *Aquificae*, a putative transcriptional regulator related to ArsR repressor, and an arsenical pump membrane protein (ArsB), both related to *Firmicutes* (see Fig. S9).

Biological sulfur species cycling in Tiger and Cub Baths. The availability and speciation of sulfur compounds within geothermal environments constrains the strategies employed by microorganisms to deal with Hg in these ecosystems. For example, Hg methylation is impeded in ecosystems with elevated aqueous sulfide concentrations (37). Conversely, the availability of soluble Hg to microorganisms is limited by the solubility and/or microbially mediated dissolution of cinnabar/metacinnabar (38). To elucidate these interactions, the Cub and Tiger Bath metagenomes were searched for genes related to dissimilatory sulfite/sulfate reduction using *dsrAB* genes that encode subunits A and B of the dissimilatory bi(sulfite) reductase enzyme (DsrAB) (39) and the *sox* pathway genes [*soxR, soxXA, soxYZ, soxB, sox(CD)$_2$, soxG*] that encode enzymes used in hydrogen sulfide and elemental sulfur oxidation (40).

Complete or near complete *dsrAB* sequences were recovered from assembled Tiger and Cub Bath metagenomes using ggKbase annotations (see Table S6). The genes were often present on scaffolds containing other genes encoding proteins involved in sulfite/sulfate reduction to sulfide. Both *dsrC* and *dsrD* genes were present on scaffolds with *dsrAB* in NW1_*Thaumarchaeota*_unknown_1, NW2_*Deltaproteobacteria*_41_12, and NW2_*Acidobacterium_capsulatum*_related. Phylogenetic analyses of the translated genes indicated six distinct groups of DsrAB sequences in Tiger and Cub Baths (Fig. 5; Table S6), groups I to VI. Three distinct groups of reductive bacterial type DsrAB groups (I to III) were identified, most closely related to known thermophilic sulfur-reducing bacteria such as *Desulfurella acetivorans* as well as uncultured *Gemmatimonas* sp. strain Sg8-17. Groups IV and V contained sequences related to reductive archaeal DsrAB in genomic bins related to *Thermoplasmata*, *Thermoplasma acidophilum*, and *Aciduliprofundum*. Group VI DsrABs contained sequences distantly related to "*Candidatus* Rokubacteria" CSP1-6, *Caldivirga maquilingensis*, and *Thermodesulfobacterium* spp. (WP_051754629). Group V DsrABs were likely uncultured reductive archaeal type DsrABs related to *Vulcanisaeta*; unbinned sequences were from scaffolds with a majority of sequences related to *Archaea*. Group VI DsrABs were most closely related (>50%) to DsrAB from the sulfate-reducer "*Candidatus* Rokubacteria" CSP1-6 (41); the sequence was distinct from DsrA of group IV and is from genomic bin NW2_*Planctomycetes*_54_12 (Table S6). The DsrAB phylogenies as represented in Fig. 5 agree with the phylogenetic annotations of the scaffolds from which the genes were obtained (Table S6). Importantly, while there is evidence for bacterial and archaeal sulfate and sulfur reduction within Tiger and Cub Baths, none of the DsrAB groups detected (groups I to VI) (Fig. 5) contain known Hg methylators from the primary sulfate-reducing phyla, *Deltaproteobacteria* and *Firmicutes* (18), and there were no *hgcAB* genes present in sulfate-reducing genomic bins from Tiger or Cub Bath.
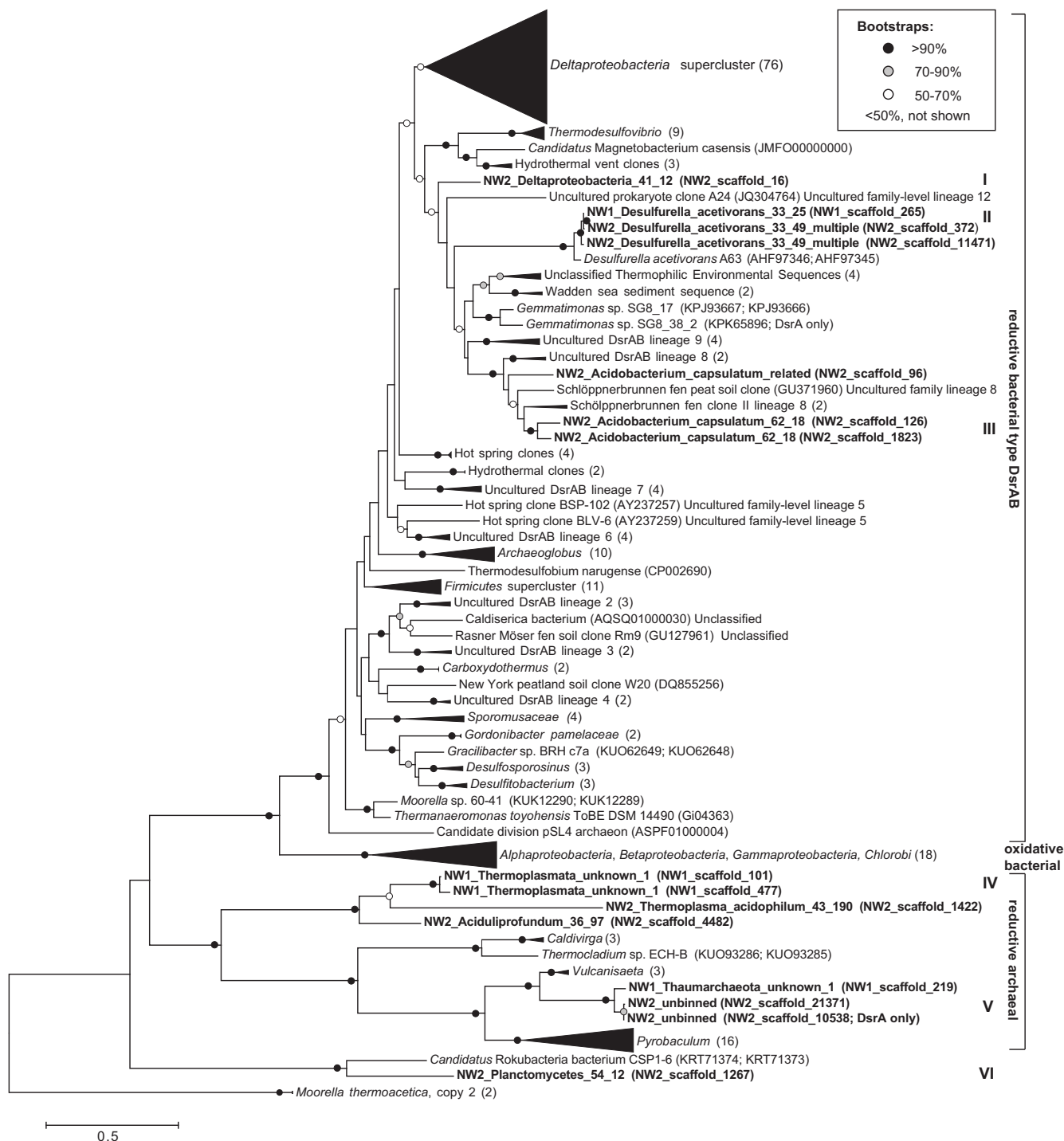
FIG 5 Phylogenetic analysis of DsrAB by maximum likelihood method. The 15 DsrAB homologues in this study were pulled from IDBA-UD assembled Tiger and Cub metagenomes using ggKbase. They were compared to 218 reference DsrAB sequences pulled from the Dome database, including 15 representative DsrAB sequences from thermophilic environments (39). There were six distinct groups of DsrAB homologues found at Ngawha. The tree was constructed using MEGA6 (77) with the Le Gascuel 2008 model with gamma distribution; pairwise distances were estimated using a JTT model. All positions with less than 95% site coverage were eliminated, including alignment gaps, missing data, and ambiguous bases. There was a total of 492 positions in the final data set, with 100 bootstrap replicates.

Genes encoding sulfur oxidation (*sox*) in acidophilic *Betaproteobacteria* and *Gammaproteobacteria* were detected in both Tiger and Cub Bath metagenomes and were related to *Acidithiobacillus* spp. and *Thiomonas* spp. (Fig. 2; Table S7). Furthermore, sequences from archaeal and bacterial *sox* pathways, including from acidophiles *Acidiphilium* and *Acidocella*, were present in the unbinned metagenomic data (Table S7).
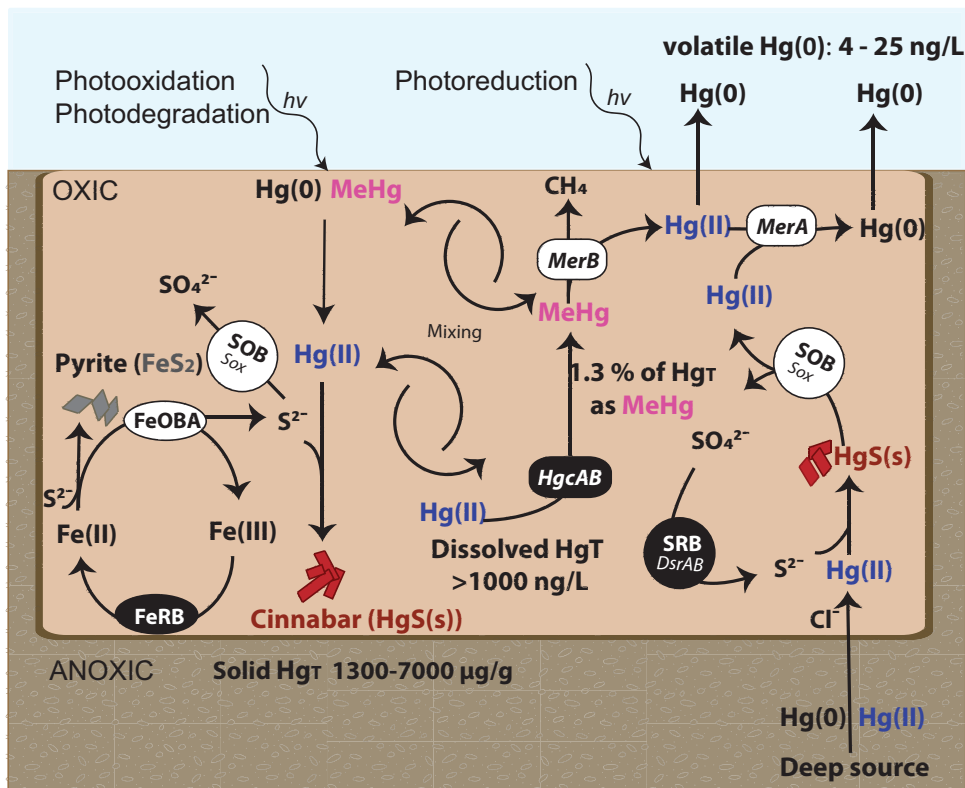
FIG 6 Conceptual model of biogeochemical cycling of mercury (Hg), sulfur (S), and iron (Fe) in Hg-enriched, sulfidic, low pH mesothermal springs. Gaseous elemental mercury [Hg(0)] [as well as Hg(II)] from deep geological sources enters the surface waters of the springs where it becomes oxidized to Hg(II) (enhanced by chloride [Cl$^-$]) (32) and then complexes with sulfides (S^{2-}) to produce cinnabar (red rhombohedral symbols; HgS$_{(s)}$). Here, S^{2-} is indicative of all reduced sulfide species. Round icons represent microbially mediated reactions, white are primarily aerobic-associated mechanisms, and black are primarily anaerobic. Sulfur-oxidizing bacteria (SOB) equipped with the Sox pathway along with Fe-oxidizing bacteria and archaea (FeOBA) are able to enhance dissolution of metal sulfides, such as pyrite (silver rhombohedral symbols; FeS$_2$) and HgS$_{(s)}$. Sulfate-reducing bacteria (SRB) and Fe-reducing bacteria (FeRB) further mediate the redox chemistry of S, Fe, and Hg. As Hg(II) becomes bioavailable to microbes, it can be reduced to Hg(0) by microbes equipped with mercuric reductase (MerA) or methylated to MeHg by HgcAB-equipped microbes. MeHg can be demethylated by MerB-equipped microbes to Hg(II) and CH, and then reduced to Hg(0) by MerA. At the surface of the springs, photoreduction can also contribute to Hg(II) reduction to Hg(0), as well as the degradation of MeHg. Photolytic oxidation may also counter Hg(0) volatilization from surface waters, keeping Hg(II) in spring water to be transformed by microbes or partitioned to sulfide minerals. Advective mixing of spring waters ensures that Hg species travel across the redox boundaries that likely partition the Mer-equipped microbes to oxic surface waters from the HgcAB-equipped microbes that likely occupy the anaerobic sediment/water boundary.

DISCUSSION

Geothermal systems provide an environment in which relationships between the chemical and physical processes controlling Hg speciation and bioavailability and microbial Hg transformations (4, 7) remain poorly understood. Temperature and pH constitute major drivers of microbial diversity in geothermal springs, with pH contributing to a greater extent (42, 43). Indeed, previous studies show that acidic geothermal spring communities appear quite distinct from those of neutral and alkali springs, irrespective of temperature (42, 43). In our study, despite their mutual close proximity and broadly similar physicochemical properties and dissolved total Hg concentrations, the Tiger and Cub Baths of the NGF hosted very distinct microbiomes (see Fig. S10 in the supplemental material). The greater diversity in genomic bins representative of the Cub Bath microbiome than of Tiger Bath (Fig. 1) may have promoted Fe and S redox cycling to a greater extent, which in turn could facilitate the dissolution of metal sulfides such as pyrite or cinnabar. Subsequently, this dissolution could have increased the bioavailability of Hg(II) for $hgcAB^+$ equipped microorganisms by oxidizing reduced S and increasing dissolved Hg(II) (Fig. 6).

NGF genomes featured similar metabolic capabilities to those recovered from AMD. The oxidation of reduced sulfur species by both aerobic and anaerobic chemolithotrophic microorganisms produces electrons utilized in respiration and CO_2 assimilation (44), critical processes for living in AMD and/or geothermal systems (44, 45). Dominant members of the Tiger Springs' communities, *Acidithiobacillus* spp. and *Thiomonas* spp., can utilize various metal- and sulfur-oxidizing enzymes, pathways, electron transport mechanisms, and substrates (44) to sustain activity. *Acidithiobacillus ferrivorans* is an obligate chemolithoautotroph and facultative anaerobe that oxidizes Fe(II); some strains are also able to utilize sulfur, thiosulfate, tetrathionate, and pyrite (46). *Acidithiobacillus ferrooxidans* can utilize metal sulfides to support growth (44), and *Acidithiobacillus caldus* is also capable of oxidizing reduced inorganic sulfur species, producing sulfate via the *sox* pathway (47). A number of other NGF genome bins, including several associated with *Thermoplasma* and *Thiomonas* spp., were equipped to respire using either sulfur or organic carbon (30), and *Thiomonas* can also oxidize arsenite [As(III)] to arsenate [As(V)] (48). The *Thiomonas*-like genome bin from Cub Bath showed evidence for the presence of both *sox* and arsenite oxidase pathways (see Fig. S2).

The microbiomes of Tiger Springs were also similar to those found in AMD with respect to stress resistance/response mechanisms for acid and heavy metals (e.g., see references 30 and 49), featuring mechanisms for pH homeostasis, for example. The highest genome coverage in each bath was associated with *Acidithiobacillus caldus*, a microorganism equipped with multiple heavy metal resistance pathways (*ars*, *mer*, *czc*, and tellurite resistance). The *mer* genes in Tiger Spring metagenomes were predominately found in aerobic bacterial and archaeal genome bins (Fig. 2; Table S5), particularly the mesophilic acidophiles *Thermoplasma* and *Acidithiobacillus* (Fig. 3). This finding was in sharp contrast to the diversity of *merA* genes in YNP metagenomic data sets, which were principally from archaeal taxa (e.g., *Sulfolobales*, *Acidilobales*, and DPANN). Based on the observations of Geesey et al. (4) that archaea dominated acid springs with high Hg content, and given that MerA homologues are often encoded in the genomes of acidophilic archaea (4, 12, 13), we expected that archaeal MerA would dominate in Tiger and Cub Baths.

While Tiger and Cub Baths are considered acidic (pH <4), they are substantially lower in temperature than springs studied in YNP and the western United States; these different observations may be due to a number of factors. First, Geesey et al. (4) noted that the number of bacterial MerA homologues detected in acid springs increases with decreasing temperature (from >73°C to <55°C). Thus, the lower temperatures at NGF may explain the presence of a larger number of bacterial MerA homologues. Second, bacterial taxa are also known to be rare in higher temperature (>65 °C) acidic (<pH 4) geothermal ecosystems (50, 51). Thus, the minimal distribution of bacteria with *mer* genes was most likely a function of low thermophilic acidophile diversity rather than the absence of a taxonomic capacity to transform Hg.

A notable feature of Cub Bath was the higher percentage of Hg_T present as $MeHg_T$ than in the Tiger Bath. We speculate that this finding reflects a greater degree of microbially mediated turnover of aqueous Hg(II) to MeHg in the former spring. However, the difference in MeHg levels between the baths could also be indicative of higher demethylation rates in Tiger Bath than in Cub Bath. While *merB* genes were identified in both baths, the sequencing coverage of *merB* scaffolds was higher in Tiger Bath (836×) than in Cub Bath (18×) (Table S5). While abiotic methylation in geothermal waters is not yet well understood (52), such processes are not likely to account for the higher MeHg levels in Cub Bath relative to those in Tiger Bath. Furthermore, NGF MeHg values were 1 to 2 orders of magnitude greater than values recorded at some YNP hot springs (5, 6). An analysis of NGF metagenomes found that *hgcA* and *hgcB* genes were only detected in Cub Bath and not Tiger Bath.

Cub Bath Hg methylation genes are most likely bacterial, belonging to a sulfate-reducing clade closely related to *Firmicutes* and *Deltaproteobacteria*, possibly from the *Nitrospirae* (Fig. S9). Microbial Hg methylation via active sulfate-reducing microorganisms is consistent with the greater observed amount of MeHg (~1.3% of dissolved total

Hg) alongside higher concentrations of reduced sulfur (3.5×) in Cub Bath. Of particular note was an $hgcAB^+$ bacterium in Cub Bath metagenome (NW2_unbinned) that may represent a novel acidophilic, possibly sulfate-reducing, Hg methylator equipped with heavy metal resistance. This genome harbored $hgcA$ and $hgcB$ on a scaffold with a putative copper chaperone (HMA/CopZ), arsenical resistance operon repressor (ArsR), and arsenical pump membrane protein (ArsB) (Fig. S9). There are few reports of arsenate reduction by sulfate-reducing bacteria (53), although putative ars genes have been found in several species of $Desulfovibrio$, $Desulfosporosinus$, $Desulfomicrobium$, and $Desulfotalea$. Genomes of known and predicted Hg-methylating bacteria and archaea, as well as closely related non-Hg-methylating bacteria and archaea, were searched for homologous proteins to those encoded on NW2_scaffold_10600 (see Table S8). Notably, ArsR family transcriptional regulators are encoded directly upstream of the genes for HgcA in $Desulfovibrio desulfuricans$ ND132 (DND132_1054) and $Desulfomicrobium$ $baculatum$ (Dbac_0377). While homologous ArsR proteins are common in genomes containing HgcA (Table S8), no genomes encode all of these proteins, although several genomes of known and predicted methylators encode copper chaperones and arsenic resistance proteins, providing a measure of confidence in genome assembly results. Notably, three homologous proteins are encoded in the genomes of $Desulfosporosinus$ spp., often found in sulfate-rich, heavy-metal-contaminated low-pH environments (54), and $Desulfosporosinus acidiphilus$, with an optimum growth pH of 3.6 to 5.5, was the first acidophile observed to methylate Hg (18). Therefore, we infer that the Cub Bath bacterium is likely a similar taxon capable of both Hg methylation and As(V) reduction.

One of the strongest influences on Hg speciation and bioavailability (for methylation or volatilization) in acidic sulfidic hot springs is the formation and dissolution of cinnabar ($HgS_{(s)}$), which in turn is impacted by the activity of sulfur- and iron-oxidizing microorganisms (5, 32, 37, 55, 56). A previous study (32) identified $HgS_{(s)}$ as the most abundant and widespread Hg-bearing mineral in the Ngawha region, an observation we confirmed by X-ray diffraction (XRD) analysis from a topsoil sample in the Tiger Springs area (Fig. S2). The observed physicochemical conditions in Tiger and Cub Baths were on the cusp of $HgS_{(s)}$ formation/dissolution, at pH 2 to 3 and pH >4 (57). Thus, the bioavailability of Hg(II) in the acid warm springs of the NGF reflected Hg solubility in the context of sulfur speciation and acidic conditions (37, 38). In aerobic sediments, sulfur- and iron-oxidizing bacteria and archaea may enhance the dissolution of cinnabar and increase Hg(II) bioavailability. Like sulfide, chloride can also affect Hg bioavailability to methylating microorganisms; methylation rates have been shown to correlate inversely with increasing chloride (Cl^-) concentration (58, 59). Chloride concentrations in Tiger Bath (470 mg liter^{-1}) were higher than those of typical freshwaters (47.9 mg liter^{-1}), and in combination with low pH, could have decreased net Hg methylation rates without impacting the viability of methylating microorganisms (58). Other factors that may influence Hg bioavailability include dissolved organic material (DOM), thiol-DOM interactions (60–62), and turbidity, which likely limits photolytic Hg transformations.

Together, these findings can account for the nearly 10× amount of filtered MeHg concentrations in Cub Bath, from which $hgcAB$ sequences were recovered, compared to that in Tiger Bath, despite their near identical Hg_T concentrations in filtered water samples and the nearly 3× higher solid Hg content of Tiger Bath. In contrast, no $hgcA$ reads were detected in the Tiger Bath metagenome at the sequencing depth of our study. Thus, bioavailable Hg may be getting enzymatically reduced or recomplexed by Hg-binding ligands (e.g., Cl^-, DOM, and S^{2-}). Indeed, the low flux of Hg(0) from the surface of the bath suggests that most of the microbially reduced Hg(II) remains dissolved and potentially is continuously cycled between Hg(0) and Hg(II) redox states. Advective mixing of anoxic and oxic waters would also promote Hg cycling and exchange between aerobes and anaerobes and, likewise, mer- and $hgcAB$-carrying microbes, in the acid warm springs (Fig. 6).

While acidophilic microbial mats in YNP have been shown to accumulate MeHg and may actively methylate Hg (5, 6), the relative difference in pHs between the two NGF springs is minimal and therefore unlikely to account for the difference in recovery of

hgcAB genes. An alternative explanation may be found in the $Hg_{(T)}$ concentration in the sediments of both springs. The total solid Hg concentration in Tiger Bath was nearly three times higher than that of Cub Bath (3,467 μg g^{-1} and 1,274 μg g^{-1}, respectively). Similarly, a small nascent hot spring located adjacent to Tiger Bath (TS3) had extremely high concentrations of both total dissolved and solid Hg (16,700 ng liter^{-1} and 7,000 μg g^{-1}, respectively). Taken together, these observations suggest that the area immediately adjacent to Tiger Bath is a highly localized Hg "hot spot," with elevated Hg levels selecting for microbial genomes encoding Hg resistance. Hg methylation capability apparently does not confer Hg(II) resistance (63), and with the exception of two *Geobacter* spp., *mer* operon genes appear to be absent in genomes of known *hgcAB$^+$* microorganisms (14, 27). These observations are further corroborated by spike-in experiments in river water sediments that showed microbial Hg methylation was inhibited by Hg concentrations as low as 15.3 μg g^{-1} (24). Another plausible control on Hg methylation in the two baths may have been temperature, which was recorded as nearly 10°C different between baths during each sampling season (Table 2). Similar differences in temperature were recorded in the sediments (Tiger Bath at 51.1 to 68.6°C and Cub Bath at 43.5 to 60.3°C). Principal-component analysis of covariance between geochemical parameters measured in all springs across the NGF (Tables 1 and 2) indicates an inverse relationship between MeHg and spring temperature (see Fig. S11). Previous work shows that known *hgcAB$^+$* methylators and predicted methylators are almost exclusively mesophiles with growth optima at ~30°C (18). Known exceptions include the thermophile and known Hg-methylator *Desulfacinum hydrothermale* (64), psychrotolerant and psychrophilic predicted methylators *Geopsychrobacter electrodiphilus* and *Methanolobus psychrophilus* R15, and a group of hyperthermophiles possessing a fused *hgcAB*-like gene of unknown methylation functionality (16).

Conceptual model of Hg speciation in warm acidic hot springs. In the NGF acid warm springs, Hg biogeochemical cycling reflects the detected or inferred microbially mediated Hg transformations as well as constraints imposed by metal sulfide solubility and vigorous microbially mediated reduced S and metal oxidation reactions. The main abiotic and biotic controls on Hg cycling in acidic mesothermal springs are depicted in the conceptual model shown in Fig. 6. The bioavailability of Hg to Mer- and HgcAB-equipped microorganisms is controlled by cinnabar precipitation and dissolution, which in turn is influenced by pH and the presence of sulfur- and iron-oxidizing and sulfate- and iron-reducing bacteria and archaea. Bioavailable Hg(II) is methylated to MeHg by microbes, putatively sulfate-reducing bacteria, equipped with HgcAB. This process is limited by demethylation of MeHg (via MerB) and reduction (via MerA) of Hg(II) to Hg(0) by facultative anaerobic and aerobic iron-cycling and sulfur-oxidizing microorganisms. The volatile Hg(0) may evolve from spring waters or be photooxidized and recycled to Hg(II). A significant sink for Hg(II) within the springs involves formation of solid HgS (metacinnabar and cinnabar) and, potentially, the adsorption of MeHg to sediments or particulate organic matter (which was not assessed here). However, under the acidic conditions, most MeHg and Hg(II) should remain dissolved and could be continuously cycled between methylating and demethylating microorganisms. Importantly, temperature (>50°C) and elevated $Hg_{(T)}$ concentrations will restrict microbial methylation of bioavailable Hg(II). However, as geothermal inputs mix with cooler water, the microbial Hg methylation potential increases. Therefore, surface waters and groundwaters that receive geothermal inputs, such as catchment waterways downgradient from NGF springs and discharges from hydrothermal power plants, may be important environmental pathways for MeHg mobilization and bioaccumulation.

MATERIALS AND METHODS

Site description. The Ngawha Geothermal Field (NGF) constituted the field site for investigating Hg cycling in a low pH (<4.5), elevated Hg (>100 ng liter^{-1}), and sulfide-rich (>0.1 mg liter^{-1}) environment (see Fig. S1 in the supplemental material). Mercury ore deposits in the NGF occur as cinnabar, metacinnabar, and native Hg(0) in association with active hot springs, fumaroles, and mud pools (65). Elemental Hg [mainly gaseous Hg(0)] travels from deep geological sources to the surface, either in hydrothermal fluids or geothermal gases, where it reacts with oxygen in the presence of chloride to form

Hg(II); Hg(II) in turn reacts with dissolved sulfide (biogenic) to precipitate cinnabar (32). Roughly 33,000 kg of cinnabar ore was mined from the Tiger Springs area at Ngawha during the first half of the 20th century (65). Tiger Springs and other areas within the NGF still host an active geothermal system that releases approximately 530 kg of Hg_T annually, ~44% of which is thought to be emitted to the atmosphere (32). The remaining Hg resides in the local surficial waters and sediments (32). Cinnabar precipitation was confirmed by X-ray diffraction analysis of Tiger Springs sediments and nearby topsoil (Fig. S2).

Sampling techniques. Several springs from three areas, Tiger Springs (TS), Ginn Ngawha Spa (GN), and Ngawha Springs Baths (NS), were sampled in April and October of 2011. Many of the springs were edged with boards for use as soaking baths. Water samples for Hg analyses were filtered through 0.45-μm membrane syringe filters, preserved with 1% (vol/vol) reagent-grade HCl, and stored in acid-washed high-density polyethylene (HDPE) bottles in the dark. Filtered water samples (0.45 μm) for anion analysis were stored in sterile 50-ml plastic Falcon tubes. All filtered samples were stored at 4°C. Redox potential (millivolts) and pH measurements were taken at each sampling site using an Orion Model 250A portable meter with a glass pH electrode; spring water temperature measurements were also taken at the time of sample collection. Sediment samples were collected from the floor or wall of each spring, as well as from bulk water samples, in sterile 50-ml Falcon tubes. The use of sediments collected on the bottom of the boarded spring bath and suspended in water allowed us to capture a mix of aerobic and anaerobic members of the microbial community as well as those that live across a range of temperatures, from the cooler waters (<45°C) to the hotter sediments (>55°C). Samples were stored on ice for ~4 days until they could be transferred to laboratory storage at −80°C (i.e., transported from New Zealand to Melbourne, Australia). Sediment samples were used for Hg_T analyses and for whole-community DNA extractions.

Hg and MeHg analyses. Total Hg and MeHg concentrations of filtered waters and freeze-dried sediments collected in April and October 2011 were measured at the Wisconsin Water Science Center (WWSC, U.S. Geological Survey, Middleton, Wisconsin) on a Perkin-Elmer Elan 9000 quadrupole inductively coupled plasma mass spectrometer (ICP-MS) and a Brooks Rand atomic fluorescence spectrophotometer model III, respectively. Filtered water samples were analyzed within 6 months of sampling at the Wisconsin Mercury Research Lab (WMRL) of the Wisconsin Water Science Center (USGS, Middleton, Wisconsin). Filtered water samples analyzed for Hg_T species were treated with a BrCl solution to ensure all Hg species in the sample were oxidized to Hg(II). Prior to analysis, $SnCl_2$ solution was added to the vials, which reduced the Hg(II) species to volatile Hg(0). The samples were then ethylated, purged with argon gas, and analyzed by gas chromatography (GC) (using Brooks Rand Autosampler and Total-Hg Purge and Trap system) in tandem with atomic fluorescence spectrometry). Methylmercury analysis of filtered waters was determined by distillation, gas chromatography separation, and speciated isotope dilution mass spectrometry using ICP-MS, according to USGS method 01–445 and WMRL standard protocols (66). Four blanks and two duplicate spikes were included in each run for quality assurance. Method detection limits for total and methylated mercury were 0.007 ng and 0.03 to 1.2 ng liter^{-1}, respectively (depending on the dilution factor required for each sample).

Sediment samples (~5 g [wet weight]) were freeze-dried overnight on a Heto-Drywinner vacuum system before shipment in sterile glass vials to the WMRL. For solid Hg_T analysis, freeze-dried samples were digested with 3:1 HCl/HNO_3 overnight in a Teflon vessel. The digested sample was then oxidized with BrCl solution. Total Hg analysis was then performed by using the same procedure as for filtered water. The detection limit for the solid Hg_T analysis was 0.2 ng. Field blanks for Hg analyses were prepared using ultrapure reaction-grade water spiked with 1% (vol/vol) ultrapure HCl stored in each type of sampling material until analysis. The Hg_T and $MeHg_T$ values for field blanks were 0.32 ng liter^{-1} and 0.57 ng liter^{-1}, respectively.

Hg(0) analysis. Vapor samples were collected in October 2011 at a height of 5 to 10 cm over Tiger and Cub Baths (Tiger Springs area) with SKC Anasorb sorbent tubes (model C300). These sorbent tubes are typically used to measure passive exposure to mercury in industrial settings (67, 68) as a flow rate of 2 liters min^{-1}. The volume of air sampled was regulated using an SKC sample air pump (PCXR4). Gas samples were passed through a soda lime trap before collection on the hopcalite sorbent to trap excess condensation and neutralize acid. Once used for sampling, sorbent tubes were sealed with Teflon tape and sent to ChemCentre (WA, Australia) to be analyzed per NIOSH method 6009. The sorbent material was dissolved and oxidized in 1:1 HNO_3/HCl. This solution was then diluted with distilled (DI) water, and immediately before analysis on a cold vapor atomic absorption spectrometer (CVAAS), 10% $SnCl_2$ was added to reduce all Hg(II) to Hg(0). This Hg(0) was then purged into the CVAAS analyzer (detection limit = 0.01 μg) in an argon gas stream. Sampling of Tiger and Cub Baths was performed under similar conditions. First, a blank Anasorb tube was exposed to ambient levels of Hg (unsealed, with no air pumped through). An additional blank, that remained sealed, was also included in analyses. Blank samples were below the method detection limit (<0.01 μg). Samples taken from the same site, with various pump times (20 to 30 min) did not yield similar adsorbed Hg concentrations. A positive correlation between total Hg adsorbed versus volume of air pumped through the adsorbent trap ($r^2 = 0.976$, $n = 4$), indicated that saturation of the adsorbent was not reached.

Common ion analysis. Common anion concentrations (F$^-$, Cl$^-$, Br$^-$, NO$_3^-$, and SO$_4^{2-}$) were measured in unacidified filtered water samples collected in April 2011 using a Dionex DX-120 ion chromatograph with an IonPAC As14 column (4 mm by 250 mm) in the Department of Chemistry at the University of Melbourne. Samples were stored in the dark at 4°C for 4 months between sample collection and analysis. The instrument was set to the following conditions: flow rate, 1.4 ml min^{-1}; eluent, 4.8 mM sodium carbonate and 0.6 mM sodium bicarbonate; injection volume, 25 μl. Chromatographs were

viewed on PeakNet Run System I software. The method detection limit for ion chromatography (IC) analyses was 0.0005 mg liter^{-1}. Concentrations were determined by a five-point calibration curve generated from Dionex Combined Seven Anion Standard I. The 5× dilution standard was run in duplicates to ensure precision of the method, and both sample and method blanks were produced using Milli-Q water at the time of sampling and during analysis, respectively. Determination of sulfide in water samples was performed on filtered water samples prepared in the field for analysis in October 2011 using the methylene blue method (69) and a Hach DR 2800 spectrophotometer (method 8131). Sulfide measurements were performed in triplicates for each sample. Total Fe was measured in filtered acidified water samples collected in October 2011 using the Ferrozine method (70) with prepared reagents coordinating with those for Hach method 8147. The method detection limit for sulfide measurements was 0.02 mg liter^{-1} and for Fe measurements was 0.5 mg liter^{-1}. The samples had been stored in the dark at 4°C prior to analysis. Sample blanks were prepared at time of sample collection using Milli-Q water.

DNA extraction. DNA was extracted from sediments collected from Tiger (TS1) and Cub (TS2) Baths and surrounding sites (TS3 and TS4) in October 2011 using the MO-BIO PowerMax DNA isolation kit, using an alteration to the manufacturer's protocol. Approximately 5 g of sediment was used for extraction. Sediments were first treated with 5 ml of 10 mM Tris-Cl (solution C6), the samples were then centrifuged at 6,000 × g for 5 min, and the supernatant was decanted. Then, bead solution C1 was added, and the alternative lysis method in the protocol was followed, which replaces the 10-min bead-beating step with incubation in a water bath at 65°C for 30 min, followed by vortexing the sample for 1 min (71). This alternative lysis method was used to reduce shearing of the DNA. Duplicate DNA extractions were performed to ensure a sufficient mass of DNA was extracted for each sample. Replicate DNA extractions were concentrated onto the same spin filter and cleaned using a QIAquick PCR purification kit (Qiagen, California).

Metagenomic analysis. Approximately 113 to 216 ng of genomic DNA extracted from samples collected in October 2011 (TS1A and TS2A) was barcoded by sample and prepared for sequencing with the NexteraXT kit, and ten samples were run on a single lane of an Illumina HiSeq 2500 with 2 × 100-bp paired-end sequencing (Australian Genome Research Facility, Melbourne, AU). This produced ~9 Gbp of sequence data for two Ngawha metagenomes, Tiger Bath (NW1) and Cub Bath (NW2), and 43 Gbp for all ten samples (Table S1). Sequences were binned by bar code, quality filtered, and trimmed to remove Illumina adapters using Trimmomatic (72). Metagenomes were examined after assembling short reads into longer contigs with IDBA-UD (73). Assembled contigs were uploaded and binned for analysis using ggKbase and have been made publicly available (http://ggkbase.berkeley.edu/).

Detection of Hg cycling genes in metagenomes. The metagenomic read sets were screened directly for sequences sharing homology with *hgcA* and *hgcB* using a hidden Markov model (HMM) method described previously (74). Metagenomic read sets were also screened directly for sequence homology with *merA* using an HMM search built previously (74). Assembled metagenomic sequences were searched for *mer* operon, *hgcA*, and *hgcB* genes using ggKbase. Genes were annotated in ggKbase by BLAST searches against the NCBI database (75). Multiple *merA* sequences were extracted from ggKbase, translated to amino acids using the bacterial translation table, and aligned using ClustalW (76) in MEGA6 (77) with MerA reference sequences from confirmed *mer* operon-possessing microorganisms (13).

Genomic binning and phylogenetic analyses. Genomic binning of metagenomic data was performed using ggKbase, based on scaffold coverage, GC content of scaffold sequences, and common taxonomy of the contigs. Bins were further refined with emergent self-organizing mapping (ESOM) (78). Scaffold coverage was calculated using Bowtie2 to map reads to the assembled sequences (79). Genome completeness was estimated from the presence of bacterial single-copy genes (51 in total) or archaeal single-copy genes (38 in total) (Table S2). Several bins, namely, NW1_*Thermoplasmata*_unknown_1, NW2_*Desulfurella_acetivorans*_33_49, and NW2_*Rhodospirillales*_68_7, are likely multigenome bins that could not be refined to single genomes from coverage and average GC splits. Information regarding genomic bins for each metagenome, as well as unbinned scaffolds, is provided in Table S2. Taxonomy was assigned to the metagenome-assembled genomes based on consensus classification of contigs. There are 34 ribosomal proteins considered universal among bacteria, archaea, and eukaryotes and which can be used to infer phylogeny (80). In this study, we used ribosomal protein S3, a single-copy gene present in every genomic bin from this study, to compare phylogenies and coverage across each metagenome-assembled genome. Ribosomal protein sequences were pulled from ggKbase and then aligned to translated ribosomal protein S3 sequences from the NCBI nonredundant protein database.

Hg cycling genes from publicly available hot spring metagenomes. To compare Hg cycling genes from NGF to those of other geothermal settings, assembled metagenomes from Yellowstone National Park (YNP) were searched for *hgcA* (Table S3) and *merA* genes (Table S4). Included in the phylogenetic analysis were HgcA protein sequences extracted from YNP metagenomic data sets (https://img.jgi.doe.gov) (Table S3). Sequences were obtained by querying all assembled hot spring metagenomic data sets for sequences sharing homology to carbon monoxide dehydrogenase (pfam03599). HgcA proteins share homology with carbon monoxide dehydrogenases and are often misannotated as such in microbial genomes (17). HgcA sequences were differentiated from carbon monoxide dehydrogenases using the HMM described above, with an inclusion value cutoff of 1E−7, and only sequences that included the conserved cap-helix region of HgcA were kept for analyses. Of a total of 234 hot spring metagenomes (of which 216 were from YNP springs) searched (as of July 2016), there were 4,520 matches to sequences annotated as carbon monoxide dehydrogenases (pfam03599) (2,148 in YNP metagenomes). Of these sequences, 102 were identified as HgcA sequences from 18 different metagenomes (Table S3). Included

in the phylogenetic analyses were 65 HgcA sequences found in 15 YNP metagenomes. The *hgcA* genes were found in YNP metagenomes sampled from four sites: Mushroom Springs (Gp0111644–45 and Gp0057794), Octopus Springs (Gp0057360, Gp0057796, Gp00111632, Gp0111634, Gp0111638, and Gp0111646), Obsidian Pool (Gp0056876), and Fairy Spring (Gp0051404). Environmental metadata were only provided for a small number of these metagenomes. Sequences from Fairy Geyser Spring (Gp0051404) are from an alkaline (pH 9 to 9.2) and mesophilic (33.3 to 36°C) phototroph-dominated mat, while sequences from Mushroom Spring (Gp0111644–45 and Gp0057794) were from the undermat layer (~3 to 5 mm) of an anoxygenic and phototrophic microbial mat in an effluent channel of the alkaline bath. The water above the mat had a recorded temperature of 60°C (81). A separate metagenomic study has reported temperature and pH measurements for Mushroom Spring (60°C, pH 8.2), Obsidian Pool (56°C, pH 5.7), and Octopus Spring (80 to 82°C, pH 7.9) (82). The additional 37 *hgcA* sequences were from assembled metagenomes sequenced from Dewar Creek Spring (77°C, pH 8.0) and Larsen North Spring, in British Columbia, Canada (83).

Data availability. The unassembled raw metagenomic sequencing data from this study are publicly available from the NCBI Sequence Read Archive (SRA). The assembled (IDBA-UD) metagenomic contigs from this study are publicly available from the NCBI Whole Genome Shotgun (WGS) project. The sequencing data can be found under the BioProject accession number PRJNA622280, with the BioSample accession numbers SAMN14506364 for the Tiger Bath and SAMN14506365 for Cub Bath metagenomes. This WGS project has been deposited at DDBJ/ENA/GenBank under the accession numbers JABEBW000000000 and JABEBX000000000.

SUPPLEMENTAL MATERIAL

Supplemental material is available online only.

SUPPLEMENTAL FILE 1, PDF file, 7.8 MB.

REFERENCES

1. Gustin MS, Lindberg SE, Weisberg PJ. 2008. An update on the natural sources and sinks of atmospheric mercury. Appl Geochem 23:482–493. https://doi.org/10.1016/j.apgeochem.2007.12.010.
2. Ball JW, McCleskey RB, Nordstrom DK, Holloway JM. 2008. Water-chemistry data for selected springs, geysers, and streams in Yellowstone National Park, Wyoming, 2003-2005. US Geological Survey, Reston, VA.
3. Mariner R, Presser T, Evans WC. 1977. Hot springs of the central Sierra Nevada, California. US Geological Survey, Reston, VA.
4. Geesey GG, Barkay T, King S. 2016. Microbes in mercury-enriched geothermal springs in western North America. Sci Total Environ 569-570: 321–331. https://doi.org/10.1016/j.scitotenv.2016.06.080.
5. King SA, Behnke S, Slack K, Krabbenhoft DP, Nordstrom DK, Burr MD, Striegl RG. 2006. Mercury in water and biomass of microbial communities in hot springs of Yellowstone National Park, USA. Appl Geochem 21:1868–1879. https://doi.org/10.1016/j.apgeochem.2006.08.004.
6. Boyd ES, King S, Tomberlin JK, Nordstrom DK, Krabbenhoft DP, Barkay T, Geesey GG. 2009. Methylmercury enters an aquatic food web through acidophilic microbial mats in Yellowstone National Park, Wyoming. Environ Microbiol 11:950–959. https://doi.org/10.1111/j.1462-2920.2008.01820.x.
7. Wang Y, Boyd E, Crane S, Lu-Irving P, Krabbenhoft D, King S, Dighton J, Geesey G, Barkay T. 2011. Environmental conditions constrain the distribution and diversity of archaeal *merA* in Yellowstone National Park, Wyoming, U.S.A. Microb Ecol 62:739–752. https://doi.org/10.1007/s00248-011-9890-z.
8. Robinson JB, Tuovinen OH. 1984. Mechanisms of microbial resistance and detoxification of mercury and organomercury compounds: physiological, biochemical, and genetic analyses. Microbiol Rev 48:95–124. https://doi.org/10.1128/MMBR.48.2.95-124.1984.
9. Schaefer JK, Yagi J, Reinfelder JR, Cardona T, Ellickson KM, Tel-Or S, Barkay T. 2004. Role of the bacterial organomercury lyase (MerB) in controlling methylmercury accumulation in mercury-contaminated natural waters. Environ Sci Technol 38:4304–4311. https://doi.org/10.1021/es049895w.
10. Simbahan J, Kurth E, Schelert J, Dillman A, Moriyama E, Jovanovich S, Blum P. 2005. Community analysis of a mercury hot spring supports occurrence of domain-specific forms of mercuric reductase. Appl Environ Microbiol 71:8836–8845. https://doi.org/10.1128/AEM.71.12.8836-8845.2005.
11. Chatziefthimiou AD, Crespo-Medina M, Wang Y, Vetriani C, Barkay T. 2007. The isolation and initial characterization of mercury resistant chemolithotrophic thermophilic bacteria from mercury rich geothermal springs. Extremophiles 11:469–479. https://doi.org/10.1007/s00792-007-0065-2.
12. Barkay T, Kritee K, Boyd E, Geesey G. 2010. A thermophilic bacterial origin and subsequent constraints by redox, light and salinity on the evolution of the microbial mercuric reductase. Environ Microbiol 12: 2904–2917. https://doi.org/10.1111/j.1462-2920.2010.02260.x.
13. Boyd E, Barkay T. 2012. The mercury resistance operon: from an origin in a geothermal environment to an efficient detoxification machine. Front Microbiol 3:349. https://doi.org/10.3389/fmicb.2012.00349.
14. Osborn AM, Bruce KD, Strike P, Ritchie DA. 1997. Distribution, diversity and evolution of the bacterial mercury resistance (*mer*) operon. FEMS Microbiol Rev 19:239–262. https://doi.org/10.1111/j.1574-6976.1997.tb00300.x.
15. Oremland RS, Culbertson CW, Winfrey MR. 1991. Methyl mercury decomposition in sediments and bacterial cultures: involvement of methanogens and sulfate reducers in oxidative demethylation. Appl Environ Microbiol 57:130–137. https://doi.org/10.1128/AEM.57.1.130-137.1991.
16. Podar M, Gilmour CC, Brandt CC, Soren A, Brown SD, Crable BR, Palumbo AV, Somenahally AC, Elias DA. 2015. Global prevalence and distribution of genes and microorganisms involved in mercury methylation. Sci Adv 1:e1500675. https://doi.org/10.1126/sciadv.1500675.

17. Parks JM, Johs A, Podar M, Bridou R, Hurt RA, Smith SD, Tomanicek SJ, Qian Y, Brown SD, Brandt CC, Palumbo AV, Smith JC, Wall JD, Elias DA, Liang L. 2013. The genetic basis for bacterial mercury methylation. Science 339:1332–1335. https://doi.org/10.1126/science.1230667.

18. Gilmour CC, Podar M, Bullock AL, Graham AM, Brown SD, Somenahally AC, Johs A, Hurt RA, Jr, Bailey KL, Elias DA. 2013. Mercury methylation by novel microorganisms from new environments. Environ Sci Technol 47:11810–11820. https://doi.org/10.1021/es403075t.

19. Liu Y-R, Yu R-Q, Zheng Y-M, He J-Z. 2014. Analysis of the microbial community structure by monitoring an Hg methylation gene (hgcA) in paddy soils along an Hg gradient. Appl Environ Microbiol 80:2874–2879. https://doi.org/10.1128/AEM.04225-13.

20. Schaefer J, Kronberg RM, Morel F, Skyllberg U. 2014. Detection of a key Hg methylation gene, hgcA, in wetland soils. Environ Microbiol Rep 6:441–447. https://doi.org/10.1111/1758-2229.12136.

21. Compeau G, Bartha R. 1985. Sulfate-reducing bacteria: principal methylators of mercury in anoxic estuarine sediment. Appl Environ Microbiol 50:498–502. https://doi.org/10.1128/AEM.50.2.498-502.1985.

22. Fleming EJ, Mack EE, Green PG, Nelson DC. 2006. Mercury methylation from unexpected sources: molybdate-inhibited freshwater sediments and an iron-reducing bacterium. Appl Environ Microbiol 72:457–464. https://doi.org/10.1128/AEM.72.1.457-464.2006.

23. Kerin EJ, Gilmour CC, Roden E, Suzuki M, Coates J, Mason R. 2006. Mercury methylation by dissimilatory iron-reducing bacteria. Appl Environ Microbiol 72:7919–7921. https://doi.org/10.1128/AEM.01602-06.

24. Chen Y, Bonzongo J, Miller G. 1996. Levels of methylmercury and controlling factors in surface sediments of the Carson River system, Nevada. Environ Pollut 92:281–287. https://doi.org/10.1016/0269-7491(95)00112-3.

25. Oremland RS, Miller LG, Dowdle P, Connell T, Barkay T. 1995. Methylmercury oxidative degradation potentials in contaminated and pristine sediments of the Carson River, Nevada. Appl Environ Microbiol 61: 2745–2753. https://doi.org/10.1128/AEM.61.7.2745-2753.1995.

26. Pak KR, Bartha R. 1998. Mercury methylation and demethylation in anoxic lake sediments and by strictly anaerobic bacteria. Appl Environ Microbiol 64:1013–1017. https://doi.org/10.1128/AEM.64.3.1013-1017.1998.

27. Lu X, Liu Y, Johs A, Zhao L, Wang T, Yang Z, Lin H, Elias DA, Pierce EM, Liang L, Barkay T, Gu B. 2016. Anaerobic mercury methylation and demethylation by Geobacter bemidjiensis Bem. Environ Sci Technol 50: 4366–4373. https://doi.org/10.1021/acs.est.6b00401.

28. Avramescu M-L, Yumvihoze E, Hintelmann H, Ridal J, Fortin D, Lean DR. 2011. Biogeochemical factors influencing net mercury methylation in contaminated freshwater sediments from the St. Lawrence River in Cornwall, Ontario, Canada. Sci Total Environ 409:968–978. https://doi.org/10.1016/j.scitotenv.2010.11.026.

29. Rytuba JJ. 2003. Mercury from mineral deposits and potential environmental impact. Environ Geol 43:326–338. https://doi.org/10.1007/s00254-002-0629-5.

30. Baker BJ, Banfield JF. 2003. Microbial communities in acid mine drainage. FEMS Microbiol Ecol 44:139–152. https://doi.org/10.1016/S0168-6496(03)00028-X.

31. EPA. 2001. Water quality criterion for the protection of human health: methylmercury: final. Office of Science and Technology, Office of Water, U.S. Environmental Protection Agency, Washington, DC.

32. Davey HA, van Moort JC. 1986. Current mercury deposition at Ngawha Springs, New Zealand. Appl Geochem 1:75–93. https://doi.org/10.1016/0883-2927(86)90039-9.

33. Yelton AP, Comolli LR, Justice NB, Castelle C, Denef VJ, Thomas BC, Banfield JF. 2013. Comparative genomics in acid mine drainage biofilm communities reveals metabolic and structural differentiation of co-occurring archaea. BMC Genomics 14:485. https://doi.org/10.1186/1471-2164-14-485.

34. Pitts KE, Summers AO. 2002. The roles of thiols in the bacterial organomercurial lyase (MerB). Biochemistry 41:10287–10296. https://doi.org/10.1021/bi0259148.

35. Gilmour CC, Bullock AL, McBurney A, Podar M, Elias DA. 2018. Robust mercury methylation across diverse methanogenic Archaea. mBio 9:e02403-17. https://doi.org/10.1128/mBio.02403-17.

36. Baker BJ, Lazar CS, Teske AP, Dick GJ. 2015. Genomic resolution of linkages in carbon, nitrogen, and sulfur cycling among widespread estuary sediment bacteria. Microbiome 3:14. https://doi.org/10.1186/s40168-015-0077-6.

37. Gilmour CC, Henry EA. 1991. Mercury methylation in aquatic systems affected by acid deposition. Environ Pollut 71:131–169. https://doi.org/10.1016/0269-7491(91)90031-Q.

38. Jew A, Behrens S, Rytuba J, Kappler A, Spormann A, Brown G, Jr. 2014. Microbially enhanced dissolution of HgS in an acid mine drainage system in the California Coast Range. Geobiology 12:20–33. https://doi.org/10.1111/gbi.12066.

39. Müller AL, Kjeldsen KU, Rattei T, Pester M, Loy A. 2015. Phylogenetic and environmental diversity of DsrAB-type dissimilatory (bi)sulfite reductases. ISME J 9:1152–1165. https://doi.org/10.1038/ismej.2014.208.

40. Friedrich CG, Bardischewsky F, Rother D, Quentmeier A, Fischer J. 2005. Prokaryotic sulfur oxidation. Curr Opin Microbiol 8:253–259. https://doi.org/10.1016/j.mib.2005.04.005.

41. Hug LA, Baker BJ, Anantharaman K, Brown CT, Probst AJ, Castelle CJ, Butterfield CN, Hernsdorf AW, Amano Y, Ise K, Suzuki Y, Dudek N, Relman DA, Finstad KM, Amundson R, Thomas BC, Banfield JF. 2016. A new view of the tree of life. Nat Microbiol 1:16048. https://doi.org/10.1038/nmicrobiol.2016.48.

42. Power JF, Carere CR, Lee CK, Wakerley GLJ, Evans DW, Button M, White D, Climo MD, Hinze AM, Morgan XC, McDonald IR, Cary SC, Stott MB. 2018. Microbial biogeography of 925 geothermal springs in New Zealand. Nat Commun 9:2876. https://doi.org/10.1038/s41467-018-05020-y.

43. Sharp CE, Brady AL, Sharp GH, Grasby SE, Stott MB, Dunfield PF. 2014. Humboldt's spa: microbial diversity is controlled by temperature in geothermal environments. ISME J 8:1166–1174. https://doi.org/10.1038/ismej.2013.237.

44. Ghosh W, Dam B. 2009. Biochemistry and molecular biology of lithotrophic sulfur oxidation by taxonomically and ecologically diverse bacteria and archaea. FEMS Microbiol Rev 33:999–1043. https://doi.org/10.1111/j.1574-6976.2009.00187.x.

45. Huber JA, Butterfield DA, Baross JA. 2003. Bacterial diversity in a subseafloor habitat following a deep-sea volcanic eruption. FEMS Microbiol Ecol 43:393–409. https://doi.org/10.1111/j.1574-6941.2003.tb01080.x.

46. Barahona S, Dorador C, Zhang R, Aguilar P, Sand W, Vera M, Remonsellez F. 2014. Isolation and characterization of a novel Acidithiobacillus ferrivorans strain from the Chilean Altiplano: attachment and biofilm formation on pyrite at low temperature. Res Microbiol 165:782–793. https://doi.org/10.1016/j.resmic.2014.07.015.

47. Chen L, Ren Y, Lin J, Liu X, Pang X, Lin J. 2012. Acidithiobacillus caldus sulfur oxidation model based on transcriptome analysis between the wild type and sulfur oxygenase reductase defective mutant. PLoS One 7:e39470. https://doi.org/10.1371/journal.pone.0039470.

48. Duquesne K, Lieutaud A, Ratouchniak J, Muller D, Lett MC, Bonnefoy V. 2008. Arsenite oxidation by a chemoautotrophic moderately acidophilic Thiomonas sp.: from the strain isolation to the gene study. Environ Microbiol 10:228–237. https://doi.org/10.1111/j.1462-2920.2007.01447.x.

49. Chen L-X, Méndez-García C, Dombrowski N, Servín-Garcidueñas LE, Eloe-Fadrosh EA, Fang B-Z, Luo Z-H, Tan S, Zhi X-Y, Hua Z-S, Martinez-Romero E, Woyke T, Huang L-N, Sánchez J, Peláez AI, Ferrer M, Baker BJ, Shu W-S. 2018. Metabolic versatility of small archaea Micrarchaeota and Parvarchaeota. ISME J 12:756–775. https://doi.org/10.1038/s41396-017-0002-z.

50. Colman DR, Poudel S, Hamilton TL, Havig JR, Selensky MJ, Shock EL, Boyd ES. 2018. Geobiological feedbacks and the evolution of thermoacidophiles. ISME J 12:225–236. https://doi.org/10.1038/ismej.2017.162.

51. Ward L, Taylor MW, Power JF, Scott BJ, McDonald IR, Stott MB. 2017. Microbial community dynamics in Inferno Crater Lake, a thermally fluctuating geothermal spring. ISME J 11:1158–1167. https://doi.org/10.1038/ismej.2016.193.

52. Nagase H, Ose Y, Sato T, Ishikawa T. 1984. Mercury methylation by compounds in humic material. Sci Total Environ 32:147–156. https://doi.org/10.1016/0048-9697(84)90127-X.

53. Barton LL, Tomei-Torres FA, Xu H, Zocco T. 2015. Metabolism of metals and metalloids by the sulfate-reducing bacteria, p 57–83. In Saffarini D (ed), Bacteria-metal interactions. Springer, Cham, Switzerland.

54. Pester M, Knorr K-H, Friedrich MW, Wagner M, Loy A. 2012. Sulfate-reducing microorganisms in wetlands–fameless actors in carbon cycling and climate change. Front Microbiol 3:72. https://doi.org/10.3389/fmicb.2012.00072.

55. Baldi F, Olson GJ. 1987. Effects of cinnabar on pyrite oxidation by Thiobacillus ferrooxidans and cinnabar mobilization by a mercury-resistant strain. Appl Environ Microbiol 53:772–776. https://doi.org/10.1128/AEM.53.4.772-776.1987.

56. Benoit JM, Gilmour CC, Mason RP, Heyes A. 1999. Sulfide controls on mercury speciation and bioavailability to methylating bacteria in sediment. Environ Sci Technol 33:951–957. https://doi.org/10.1021/es9808200.

57. Barnett MO, Harris LA, Turner RR, Stevenson RJ, Henson TJ, Melton RC,

Hoffman DP. 1997. Formation of mercuric sulfide in soil. Environ Sci Technol 31:3037–3043. https://doi.org/10.1021/es960389j.

58. Barkay T, Gillman M, Turner RR. 1997. Effects of dissolved organic carbon and salinity on bioavailability of mercury. Appl Environ Microbiol 63:4267–4271. https://doi.org/10.1128/AEM.63.11.4267-4271.1997.

59. Boyd ES, Yu R-Q, Barkay T, Hamilton TL, Baxter BK, Naftz DL, Marvin-DiPasquale M. 2017. Effect of salinity on mercury methylating benthic microbes and their activities in Great Salt Lake, Utah. Sci Total Environ 581–582:495–506. https://doi.org/10.1016/j.scitotenv.2016.12.157.

60. Moreau JW, Gionfriddo CM, Krabbenhoft DP, Ogorek JM, DeWild JF, Aiken GR, Roden EE. 2015. The effect of natural organic matter on mercury methylation by *Desulfobulbus propionicus* 1pr3. Front Microbiol 6:1389. https://doi.org/10.3389/fmicb.2015.01389.

61. Graham AM, Aiken GR, Gilmour CC. 2012. Dissolved organic matter enhances microbial mercury methylation under sulfidic conditions. Environ Sci Technol 46:2715–2723. https://doi.org/10.1021/es203658f.

62. Ndu U, Christensen GA, Rivera NA, Gionfriddo CM, Deshusses MA, Elias DA, Hsu-Kim H. 2018. Quantification of mercury bioavailability for methylation using diffusive gradient in thin-film samplers. Environ Sci Technol 52:8521–8529. https://doi.org/10.1021/acs.est.8b00647.

63. Gilmour CC, Elias DA, Kucken AM, Brown SD, Palumbo AV, Schadt CW, Wall JD. 2011. Sulfate-reducing bacterium *Desulfovibrio desulfuricans* ND132 as a model for understanding bacterial mercury methylation. Appl Environ Microbiol 77:3938–3951. https://doi.org/10.1128/AEM.02993-10.

64. Malcolm EG, Schaefer JK, Ekstrom EB, Tuit CB, Jayakumar A, Park H, Ward BB, Morel FM. 2010. Mercury methylation in oxygen deficient zones of the oceans: no evidence for the predominance of anaerobes. Mar Chem 122:11–19. https://doi.org/10.1016/j.marchem.2010.08.004.

65. Christie T, Brathwaite B. 2002. Mineral commodity report 8: mercury, p 32. Institute of Geological and Nuclear Sciences Ltd., Lower Hutt, New Zealand.

66. Olson ML, DeWild JF. 1999. Techniques for the collection and species-specific analysis of low levels of mercury in water, sediment, and biota, p 191–200. *In* Morganwalp DW, Buxton HT (ed), U.S. Geological Survey Toxic Substances Hydrology Program—Proceedings of the Technical Meeting, Charleston, South Carolina, March 8–12, 1999—Volume 2 of 3—Contamination of Hydrologic Systems and Related Ecosystems: U.S. Geological Survey Water-Resources Investigations Report 99–4018. US Geological Survey, Reston, VA.

67. Takaya M, Joeng JY, Ishihara N, Serita F, Kohyama N. 2006. Field evaluation of mercury vapor analytical methods: comparison of the "double amalgam method" and ISO 17733. Ind Health 44:287–290. https://doi.org/10.2486/indhealth.44.287.

68. Gionfriddo C, Ogorek J, Butcher M, Krabbenhoft D, Moreau J. 2015. Mercury distribution and mobility at the abandoned Puhipuhi mercury mine, Northland, New Zealand. N Z J Geol Geophys 58:78–87. https://doi.org/10.1080/00288306.2014.979840.

69. Cline JD. 1969. Spectrophotometric determination of hydrogen sulfide in natural waters 1. Limnol Oceanogr 14:454–458. https://doi.org/10.4319/lo.1969.14.3.0454.

70. Stookey LL. 1970. Ferrozine—a new spectrophotometric reagent for iron. Anal Chem 42:779–781. https://doi.org/10.1021/ac60289a016.

71. Zhou J, Bruns MA, Tiedje JM. 1996. DNA recovery from soils of diverse composition. Appl Environ Microbiol 62:316–322. https://doi.org/10.1128/AEM.62.2.316-322.1996.

72. Bolger AM, Lohse M, Usadel B. 2014. Trimmomatic: a flexible trimmer for Illumina sequence data. Bioinformatics 30:2114–2120. https://doi.org/10.1093/bioinformatics/btu170.

73. Peng Y, Leung HC, Yiu S-M, Chin FY. 2012. IDBA-UD: a de novo assembler for single-cell and metagenomic sequencing data with highly uneven depth. Bioinformatics 28:1420–1428. https://doi.org/10.1093/bioinformatics/bts174.

74. Gionfriddo CM, Tate MT, Wick RR, Schultz MB, Zemla A, Thelen MP, Schofield R, Krabbenhoft DP, Holt KE, Moreau JW. 2016. Microbial mercury methylation in Antarctic sea ice. Nat Microbiol 1:16127. https://doi.org/10.1038/nmicrobiol.2016.127.

75. Altschul SF, Gish W, Miller W, Myers EW, Lipman DJ. 1990. Basic local alignment search tool. J Mol Biol 215:403–410. https://doi.org/10.1016/S0022-2836(05)80360-2.

76. Larkin MA, Blackshields G, Brown NP, Chenna R, McGettigan PA, McWilliam H, Valentin F, Wallace IM, Wilm A, Lopez R, Thompson JD, Gibson TJ, Higgins DG. 2007. ClustalW and ClustalX version 2. Bioinformatics 23:2947–2948. https://doi.org/10.1093/bioinformatics/btm404.

77. Tamura K, Stecher G, Peterson D, Filipski A, Kumar S. 2013. MEGA6: Molecular Evolutionary Genetics Analysis version 6.0. Mol Biol Evol 30:2725–2729. https://doi.org/10.1093/molbev/mst197.

78. Ultsch A, Mörchen F. 2005. ESOM-Maps: tools for clustering, visualization, and classification with Emergent SOM. University Marburg, Marburg, Germany.

79. Langmead B, Salzberg SL. 2012. Fast gapped-read alignment with Bowtie 2. Nat Methods 9:357–359. https://doi.org/10.1038/nmeth.1923.

80. Yutin N, Puigbò P, Koonin EV, Wolf YI. 2012. Phylogenomics of prokaryotic ribosomal proteins. PLoS One 7:e36972. https://doi.org/10.1371/journal.pone.0036972.

81. Thiel V, Wood JM, Olsen MT, Tank M, Klatt CG, Ward DM, Bryant DA. 2016. The dark side of the mushroom spring microbial mat: life in the shadow of chlorophototrophs. I. Microbial diversity based on 16S rRNA gene amplicons and metagenomic sequencing. Front Microbiol 7:919. https://doi.org/10.3389/fmicb.2016.00919.

82. Inskeep WP, Jay ZJ, Tringe SG, Herrgard M, Rusch DB, YNP Metagenome Project Steering Committee and Working Group Members. 2013. The YNP metagenome project: environmental parameters responsible for microbial distribution in the Yellowstone geothermal ecosystem. Front Microbiol 4:67. https://doi.org/10.3389/fmicb.2013.00067.

83. Eloe-Fadrosh EA, Paez-Espino D, Jarett J, Dunfield PF, Hedlund BP, Dekas AE, Grasby SE, Brady AL, Dong H, Briggs BR, Li W-J, Goudeau D, Malmstrom R, Pati A, Pett-Ridge J, Rubin EM, Woyke T, Kyrpides NC, Ivanova NN. 2016. Global metagenomic survey reveals a new bacterial candidate phylum in geothermal springs. Nat Commun 7:10476. https://doi.org/10.1038/ncomms10476.

84. Hoggins FE, Brooks RR. 1973. Natural dispersion of mercury from Puhipuhi, northland, New Zealand. N Z J Mar Freshwater Res 7:125–132. https://doi.org/10.1080/00288330.1973.9515459.

85. Krabbenhoft D, Engstrom D, Gilmour C, Harris R, Hurley J, Mason R. 2007. Monitoring and evaluating trends in sediment and water indicators, p 47–87. *In* Murray MW, Saltman T, Harris R, Mason R, Reash R, Krabbenhoft DP (ed), Ecosystem responses to mercury contamination: indicators of change. CRC Press, Boca Raton, FL.